Eur. Phys. J. C (2026) 86:565
https://doi.org/10.1140/epjc/s10052-026-15788-9

THE EUROPEAN PHYSICAL JOURNAL C

Regular Article - Theoretical Physics

Einstein–Aether primordial universe with radiation and dark energy

A. Oliveira Castro Junior[1,a], **G. A. Monerat**[1,b], **G. Oliveira-Neto**[2,c], **E. V. Corrêa Silva**[3,d]

[1] Departamento de Modelagem Computacional, Instituto Politécnico, Universidade do Estado do Rio de Janeiro, 28625-570 Nova Friburgo, RJ, Brazil
[2] Departamento de Física, Instituto de Ciências Exatas, Universidade Federal de Juiz de Fora, 36036-330 Juiz de Fora, Minas Gerais, Brazil
[3] Departamento de Matemática, Física e Computação, Faculdade de Tecnologia, Universidade do Estado do Rio de Janeiro, 27537-000 Resende, RJ, Brazil

Received: 28 January 2026 / Accepted: 30 April 2026

Abstract We investigate a quantum cosmological model within the framework of Einstein–Aether gravity. The model consists of a positively curved FLRW Universe whose matter content is described by a radiation fluid, in the presence of a positive cosmological constant Λ. We first perform a classical Hamiltonian analysis, constructing the phase space and deriving the dynamics of the scale factor. Notably, we identify specific initial conditions that lead to an inflationary expansion. Subsequently, we quantize the model following Dirac's formalism, obtaining the Wheeler-DeWitt equation for the wave function of the Universe. We solve this equation numerically and compare our results to those of the WKB approximation, computing quantum tunneling probabilities and the expectation value of the scale factor, along with its standard deviation. Finally, we analyze how these tunneling probabilities are influenced by variations in the fundamental parameters of the theory (Λ, σ, β) and the energy of the fluid E. Our results indicate a higher probability for the quantum birth of the Universe in a parameter regime characterized by larger values of Λ, σ, and fluid energy E, together with a smaller value of β.

1 Introduction

General Relativity states that our Universe starts in the event called *Big Bang*. The existence of this initial singularity leads to fundamental inconsistencies in the portrayal of the first moments of the Universe, because General Relativity loses its predictive powers at that specific event. A quantum theory of gravity is necessary to understand them. Quantum Cosmology emerges in this scenario to describe the Universe as a whole through quantum theory. It aims mainly at issues like the initial singularity or spacetime initial conditions [1–3].

The Arnowitt, Deser and Misner(ADM) formalism brought an important geometrical interpretation for the Hamiltonian formulation of General Relativity [4] by describing the Universe dynamics as the time evolution of the induced metric over a 3-dimensional hypersurface immersed in the 4-dimensional spacetime. The quantization of General Relativity using Dirac's formalism leads to the Wheeler-DeWitt equation [5,6], which governs the wave function of the Universe, which is treated as a quantum system the dynamical variables of which are associated to the geometry of spacetime [5,7]. It comes as an attempt to get rid of the singularities found in General Relativity's cosmological solutions [8] using the quantum tunneling as central mechanism known as *the spontaneous creation of the Universe from nothing* [9], stating that the birth of the early Universe depends only on the quantum nature of the theory. Quantum Cosmology also brings some tools to study the early Universe through toy models.

Besides the quantum tunneling approach, other scenarios such as cosmic bounce models [10] have also been investigated as alternatives to avoid the initial singularity. In addition, the inflationary phase of the Universe has been extensively studied in the context of modified gravity theories, such as $f(R)$ gravity [11], where the aim is to achieve consistency with the latest data from the Atacama Cosmology Telescope (ACT) and the Planck mission. Integrable cosmological models, often associated with Painlevé equations,

[a] e-mail: alessandro.castro@iprj.uerj.br (corresponding author)
[b] e-mail: monerat@uerj.br
[c] e-mail: gilneto@fisica.ufjf.br
[d] e-mail: profeduvasquezuerj@gmail.com.br

Published online: 22 May 2026

also offer valuable insights into the nature of dark energy [12], complementing the phenomenological analysis of theories such as Einstein–Aether.

The probability of Lorentz symmetry breaking at certain energy scales [13] has awoken some interest in gravitational theories incorporating this phenomenon, such as Einstein–Aether (EA) theory [14,15]. This theory consists in a change in General Relativity where one inserts a unitary timelike vector field u^a which sets a locally preferred reference frame at each point of spacetime. Lorentz symmetry breaking also implies possible reconsiderations of several subjects such as dark matter and dark energy, cosmic microwave background and cosmic inflation [16–18].

In this context, other modified gravity theories have been explored to explain late-time cosmic acceleration, such as $f(T, L_m)$ gravity [19], $f(R)$ gravity [11], $f(R, \Sigma, T)$ gravity [20], $f(Q)$ gravity [10], and $F(T, T_G)$ gravity [21]. These models often seek to provide a unified description of cosmic evolution without resorting to a cosmological constant. Rigorous observational constraints on these models, using data from supernovae, baryon acoustic oscillations, and the cosmic microwave background (CMB), have been obtained through techniques such as Hubble parameter reconstruction [22], which has become an essential tool for validating these alternative theories.

The main motivation behind the choice of EA theory is the abundance of recent works based on this theory. Using data from the Event Horizon Telescope (EHT), researchers were able to find a black hole solution using EA gravity that agrees with the shadow size of the EHT M87* [23] within certain ranges for the parameters of the model. Bairagi [24] constructs a cosmological model within the framework of EA gravity, incorporating a non-canonical scalar field as dark energy. The model's viability is assessed by comparing its predictions against Type Ia supernovae data from the Union2.1, JLA, and Pantheon compilations. The analysis demonstrates that the model provides a good fit to the observational data and successfully accounts for the Universe's accelerated expansion. By analyzing the electrodynamics and plasma magnetosphere of a magnetized neutron star, Bokhari et al. [25] derived novel observational constraints on the parameter space of EA theory. Their work, which incorporates both vacuum and plasma physics, places stringent upper limits on the theory's fundamental parameters. Adam et al. [26] numerically constructed stationary and rotating black hole solutions in EA theory, investigating two phenomenologically viable regions of the parameter space characterized by large coupling constants. Despite the potential for significant deviations from General Relativity in those regimes, their central finding is that the rotating solutions converge remarkably well to the Kerr metric. This behavior is attributed to the aether field dynamically configuring itself into a state that is either nearly torsion-free or free of both torsion and expansion. Reference [27] investigates axial gravitational perturbations of a uniform-density star within scalar-EA theory, demonstrating that a nontrivial scalar profile is unsustainable, as it induces a central divergence upon applying the Israel junction conditions for a minimally coupled scalar field. Furthermore, the authors establish that a stellar radius smaller than the peak of the vacuum Schwarzschild-type effective potential leads to the formation of a trapping well, giving rise to an echo phenomenon in the axial gravitational wave signal. In Reference [28], the equations of motion for compact binary systems are derived within EA theory, extending it to the calculation of gravitational radiation reaction effects, and achieving a precision comparable to the quadrupole approximation in General Relativity.

Throughout this work, we studied a quantum cosmological de-Sitter model described by the FLRW metric whose matter content is described by a radiation fluid (a perfect fluid with equation of state $p = \omega\rho$, in which $\omega = 1/3$) and dark energy, represented by the cosmological constant Λ [29]. The choice of a positive-valued cosmological constant is largely supported by the literature [30–33].

This work is structured as follows. Section 2 shows the classical version of the model. We consider a FLRW isotropic and homogeneous Universe, and build its Hamiltonian and the correspoding Hamilton equations of motion in the phase space. By numerically solving the equation for the scale factor we find solutions that match the phase space predictions. We then show how this model can emulate the results of cosmic inflation. In Sect. 3 we quantize the model following Dirac's formalism. We build the Wheeler-DeWitt equation for the model and solve it numerically (using the finite-differences Crank-Nicolson scheme). Subsequently, we compute the expectation value for the scale factor and its related uncertainty. In Sect. 4 we analyze the behavior of tunneling probabilities as one varies the theory parameters as well as the fluid energy, comparing those results with the ones from the WKB approximation. Section 5 is dedicated to our conclusions. Appendix A details how the Hamiltonian of our model is obtained from the total action. Appendix B examines the observational constraints on the coupling constants of the model. Appendix C details the numerical solution of the Wheeler-DeWitt equation throught the Crank-Nicolson scheme. Appendix D analyzes the self-adjointness of the Hamiltonian operator. Finally, appendix E presents the WKB approximation used for comparisons of the tunneling probability.

2 Classical model

2.1 The Einstein–Aether action and minisuperspace reduction

The total action, which generalizes the Einstein–Hilbert action and includes the EA action [34] and the matter content,reads

$$S = \frac{1}{16\pi G}\left[\int_{\mathcal{M}} d^4x\sqrt{-g}\ \left(R + \lambda(u^\mu u_\mu + 1) - K^{\rho\sigma}_{\mu\nu}\nabla_\rho u^\mu \nabla_\sigma u^\nu\right)\right] + \int_{\mathcal{M}} d^4x\sqrt{-g}\ p + \frac{1}{8\pi G}\int_{\partial\mathcal{M}} d^3x\sqrt{h}\ h^{ab}B_{ab}, \quad (1)$$

featuring an explicit unit timelike vector field u, known as the *aether field*, which violates the Lorentz symmetry by defining a preferred direction in spacetime at each point of the domain $\mathcal{M}$ while maintaining the general covariance of the theory. Here, G is the gravitational constant; g is the determinant the spacetime metric $g_{\mu\nu}$; R is the curvature scalar derived from the latter; λ is a Lagrange multiplier for the normalization and time-like character on the aether field, i.e., $u^\mu u_\mu = -1$. The tensor $K^{\mu\nu}_{\rho\sigma}$ contains the coupling constants of the model,

$$K^{\rho\sigma}_{\mu\nu} = c_1\, g^{\rho\sigma} g_{\mu\nu} + c_2\, \delta^\rho_\mu \delta^\sigma_\nu + c_3\, \delta^\rho_\nu \delta^\sigma_\mu + c_4\, u^\rho u^\sigma g_{\mu\nu}, \quad (2)$$

in which the dimensionless coefficients c_i's couple the aether field to the metric. Moreover, p is the pressure of the perfect fluid, representing the matter content; h is the determinant of the induced 3-metric h_{ab} on the boundary $\partial\mathcal{M}$ of $\mathcal{M}$, and B_{ab} is the extrinsic curvature. The integral over $\partial\mathcal{M}$ is a surface term and does not affect the equations of motion, so it will be ignored. In this work, we will use natural units $c = \hbar = 8\pi G = 1$.

The matter content of the model, introduced through Schutz formalism [35–37], is a perfect isotropic fluid with equation of state of the form

$$p = \omega\rho, \quad (3)$$

which relates the fluid's pressure p to the energy density ρ. The parameter ω determines the type of fluid under consideration; for a radiation fluid, $\omega = 1/3$. Its energy-momentum tensor reads

$$T_{\mu\nu} = (\rho + p)U_\mu U_\nu - p g_{\mu\nu}, \quad (4)$$

in which U_μ is the timelike four-velocity of the fluid. In comoving coordinates, $U^\mu = \delta^\mu_0$.

In its turn, a cosmological constant Λ is equivalent to a perfect fluid with equation of state (3) and $\omega = -1$.

The classical model is built considering an isotropic and homogeneous Universe, described by the FLRW metric

$$ds^2 = -N^2(t)\,dt^2 + a^2(t)\left[\frac{dr^2}{1-kr^2} + r^2(d\theta^2 + \sin^2\theta\, d\phi^2)\right], \quad (5)$$

in which t is the cosmological time, $a(t)$ is the scale factor, $N(t)$ is the lapse function and the parameter k determines the curvature of the spatial geometry of the Universe: open ($k = -1$), closed ($k = 1$) or flat ($k = 0$). In this work, we assume a positive curvature ($k = 1$).

By choosing $N(t) = a(t)$ and introducing the conformal time η so that

$$dt = a(\eta)\, d\eta, \quad (6)$$

we obtain the total Hamiltonian

$$H = \frac{p_a^2}{2m} + V(a) - p_T, \quad (7)$$

in which p_a is the momentum canonically conjugate to the scale factor a, T is the degree of freedom associated to the material fluid, and p_T its corresponding momentum. For the derivation of the classical Hamiltonian (7), the reader is referred to appendix A. The effective potential $V(a)$ reads

$$V(a) = \frac{m\omega_k^2 a^2}{2} - \Lambda a^4, \quad (8)$$

in which the parameters m and ω_k are defined as

$$m = \frac{6(\beta+2)}{\sigma}, \quad \text{and} \quad \omega_k = \sqrt{\frac{2k}{\beta+2}}, \quad (9)$$

and β and σ are combinations of the EA coupling constants. In this work, we let $\Lambda = 0.05$, $\beta = 0.27$ and $\sigma = 0.9999$, unless stated otherwise. This choice of values, albeit somewhat arbitrary, must take several constraints of the model into account. The relations among β, σ and the coupling constants c_i's of (2), and the observational constraints upon the c_i's can be found in Appendix B. The shape of the potential, for the aforementioned values of β and σ, is shown in Fig. 1.

2.2 Hamilton equations and the phase space

Hamilton's equation for the canonical variables (a, p_a, T, p_T) read

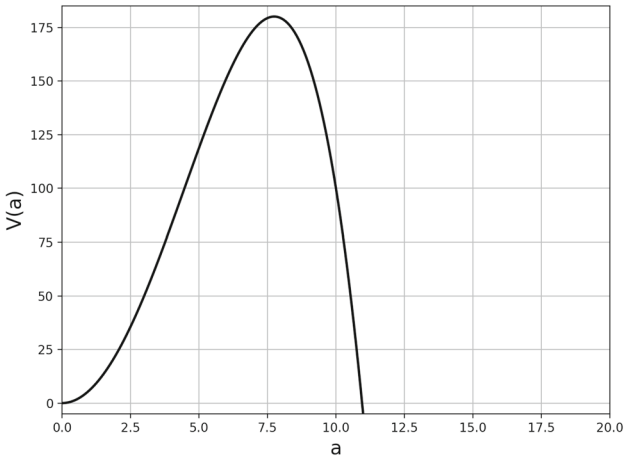

Fig. 1 The effective potential $V(a)$, defined in Eq. (8). Here, we let $\beta = 0.27$, $\Lambda = 0.05$ and $\sigma = 0.9999$

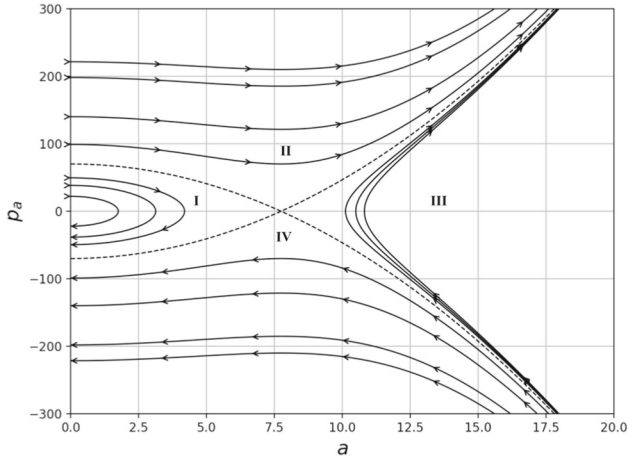

Fig. 2 Orbits in the (a, p_a) plane of the classical model's phase space, divided into four different regions of qualitatively distinct behavior: (I) Big Crunch; (II) expansion; (III) bounce; and (IV) contraction. The dotted boundary lines between adjacent regions are called separatrices

$$\begin{cases} \dot{a} = \frac{\partial H}{\partial p_a} = \frac{p_a}{m}, \\ \dot{p}_a = -\frac{\partial H}{\partial a} = -4\Lambda a^3 - m\omega_k a, \\ \dot{T} = \frac{\partial (NH)}{\partial p_T} = -1, \\ \dot{p}_T = -\frac{\partial (NH)}{\partial T} = 0, \end{cases} \tag{10}$$

in which the dot represents the derivative with respect to the conformal time η (and $N(a) = a(\eta)$). After manipulating Hamilton equations (10), one finds a second-order differential equation for the scale factor,

$$\frac{d^2 a(\eta)}{d\eta^2} = \frac{4\Lambda}{m} a(\eta)^3 - \omega_k^2 a(\eta). \tag{11}$$

According to the initial conditions that are chosen, four sets of qualitatively distinct solutions are obtained, corresponding to four distinct regions of the (a, p_a) plane, as shown in Figs. 2: (I) Big Crunch; (II) expansion; (III) bounce; and (IV) contraction. Each boundary between two distinct regions, represented in Fig. 2 as dotted lines, is called a *separatrix*. Figure 3 exemplifies the typical behavior of a solution, in each group. Solving numerically Eq. (11) for $a(0) = 0.1$ and $\dot{a}(0) = 5.0$ yields a Big Crunch solution (region I); for $a(0) = 2.0$ and $\dot{a}(0) = 100.0$ we obtain an expansive solution (region II); for $a(0) = 20.0$ and $\dot{a}(0) = -25.0$, one gets a bouncing solution (region III); and, finally, for $a(0) = 12.0$ and $\dot{a}(0) = -250.0$ we obtain a contracting solution (region IV).

2.3 On the inflationary behavior

In the early 80's the concept of Cosmic Inflation was introduced to explain some disparities between theoretical predictions and observational data, as well as to clarify some theoretical problems [38–40]. It essentially states that an exponential growth occurred in the very early Universe, after which it continued to expand, but at a slower rate. In 1929, Edwin Hubble's observations of the expansion of Universe led to Hubble's law: galaxies are moving away from one another with speed proportional to their distance. Therefore, we use this piece of information to scrutinize our model, searching for some configuration that might match the observational data available: that inflation took place from about $10^{-36}s$ to $10^{-32}s$ after the Big Bang, with the exponential expansion of the Universe by a factor of about 10^{26}. In Fig. 2, regions II and III correspond to expanding and bouncing solutions, respectively. We then seek for initial conditions in those regions that might lead to exponential growth of the scale factor, compatible with known data: a ratio of $\sim 10^4$ between the final and the initial moments of the inflationary period, an expansion rate of the scale factor of $\sim 10^{26}$, and a number of e-folds [41]

$$D = ln\left(\frac{a_f}{a_i}\right) \approx 60. \tag{12}$$

Table 1 shows several examples of initial conditions and corresponding time intervals yielding expansion ratios $\sim 10^{26}$. We have expressed our time intervals in terms of the conformal time η and also the cosmological time t.

2.4 The Hubble parameter

The *Hubble parameter* [42–44] is defined as a function of the cosmological time t as

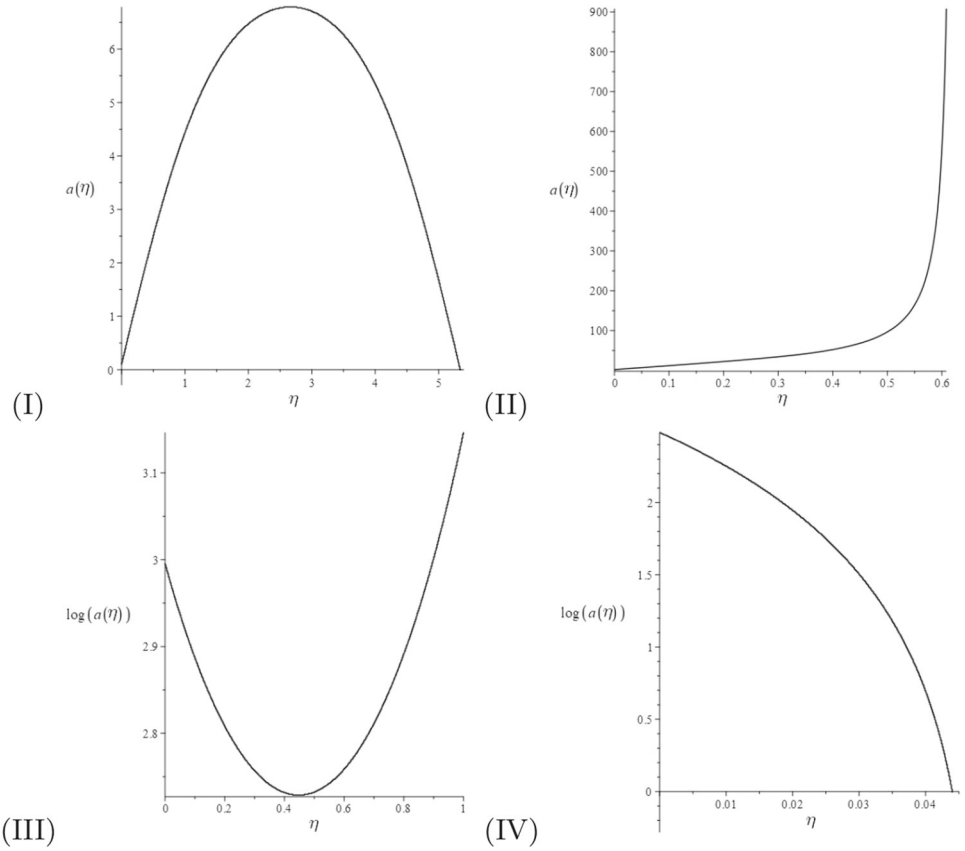

Fig. 3 Examples of classical solutions for the scale factor, in correspondence to the phase plane regions shown in Fig. 2: (I) Big Crunch, (II) expansion, (III) bounce and (IV) contraction

Table 1 Sets of initial conditions compatible with the order of magnitude of the inflationary expansion ratio and number of e-folds

Initial Conditions a, p_a	Conformal Time η	Cosmological Time t	Expansion Ratio a_f/a_i	Number of e-folds
$a(0) = 0.09$	$\eta_i = 0.01$	$t_i = 0.5743951$	$1.0096030687003838 \times 10^{26}$	59.87676967016636
$p_a(0) = 190.0$	$\eta_f = 1000$	$t_f = 2.00873$		
$a(0) = 2.0$	$\eta_i = 0.001$	$t_i = 0.3548526$	$5.316494988828418 \times 10^{26}$	61.53802666738409
$p_a(0) = 100.0$	$\eta_f = 100.0$	$t_f = 1.114255$		
$a(0) = 16.0$	$\eta_i = 0.001$	$t_i = 0.7773874$	$8.29144989079858 \times 10^{26}$	61.98243726805669
$p_a(0) = -10.0$	$\eta_f = 100.0$	$t_f = 1.323167$		

$$H_b(t) \equiv \frac{\dot{a}(t)}{a(t)}. \tag{13}$$

The *deceleration parameter* [44], in its turn, as

$$q(t) \equiv -\frac{\ddot{a}(t)\, a(t)}{\dot{a}(t)^2}, \tag{14}$$

which leads to

$$\dot{H}_b = -H_b^2(1+q) \quad \longleftrightarrow \quad q = -\left(\frac{\dot{H}_b}{H_b^2} + 1\right), \tag{15}$$

in which the dot indicates derivative w.r.t. t. According to the ΛCDM model, $q \to -1$ as the cosmological constant Λ becomes dominant over matter, which means that $\dot{H}_b \to 0$; hence the Hubble parameter H_b tends to a constant value and the scale factor of the Universe will grow exponentially in time. Figure 4 exemplifies two cases from Table 1, from the expansion and bouncing solution regions, respectively. Both remain constant over the time interval during which the exponential growth takes place (Fig. 5).

In terms of the conformal time η (cf. Eq. (6)), the Hubble and the deceleration parameters get the form

$$H_b(\eta) = \frac{1}{a(\eta)^2}\frac{da(\eta)}{d\eta} \tag{16}$$

and

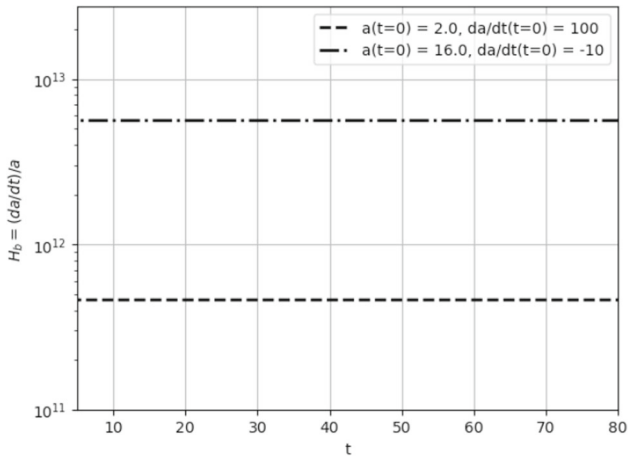

Fig. 4 The Hubble parameter H_b as a function of the cosmological time t. It remains constant during the whole inflation period

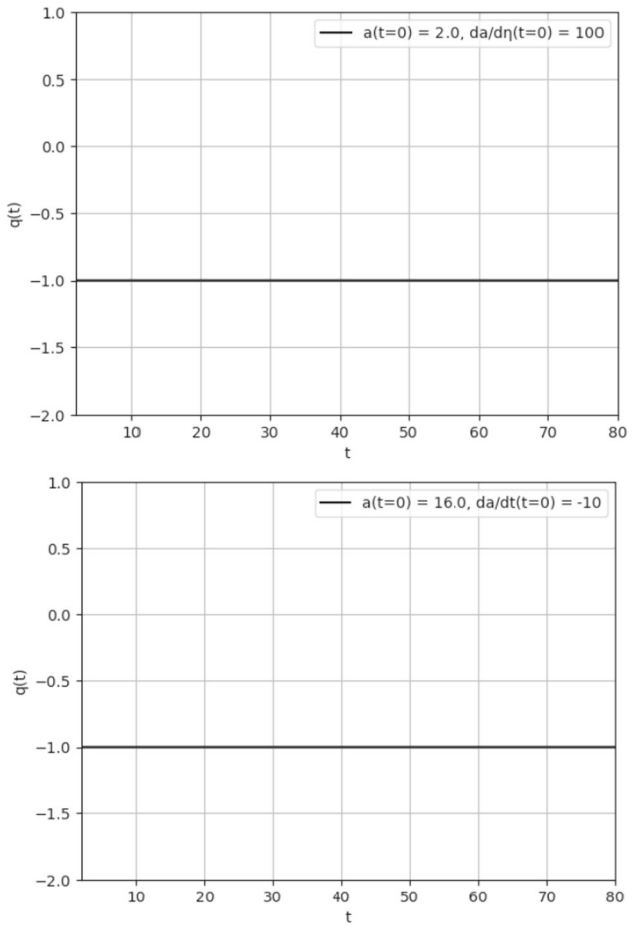

Fig. 5 Deceleration parameter q as a function of the cosmological time t for the same two initial conditions shown in Fig. 4, leading to inflation

$$q(\eta) = 2\,a(\eta) - \frac{a(\eta)^2}{\left(\frac{da(\eta)}{d\eta}\right)^2}\frac{d^2a(\eta)}{d\eta^2} - 1 \tag{17}$$

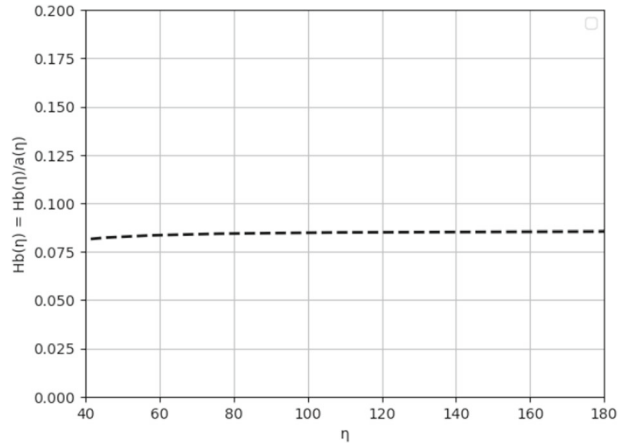

Fig. 6 The Hubble parameter H_b as a function of the conformal time η. It remains constant during the whole inflation period

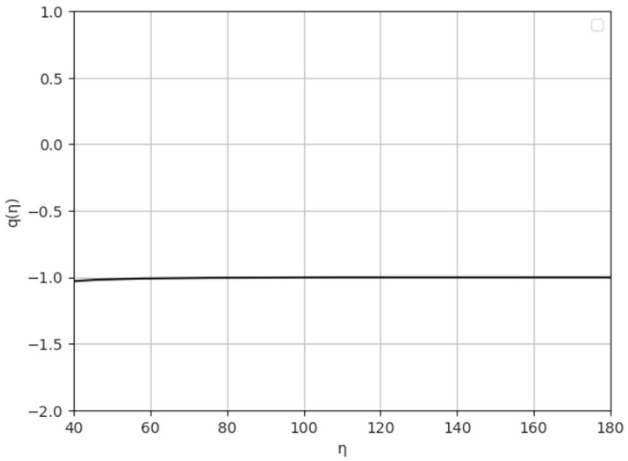

Fig. 7 Deceleration parameter q as a function of the conformal time η for one of the two initial conditions shown in Fig. 4, leading to inflation

respectively. Their behavior is the same as in the cosmological time; an example is given in Figs. 6 and 7.

3 The quantum model

3.1 Canonical quantization and Wheeler–DeWitt equation

We quantize the theory, following Dirac's formalism, by promoting the variables (a, T) to operators, together with their respective canonical momenta [45,46],

$$\hat{p}_a \to -i\frac{\partial}{\partial a} \quad \text{and} \quad \hat{p}_T \to -i\frac{\partial}{\partial T}\ , \tag{18}$$

under the fundamental commutation relations

$$[a, T] = 0\ ,\ [p_a, p_T] = 0 \ \text{ and } \ [a, p_a] = [T, p_T] = i\ . \tag{19}$$

Then from the classical constraint $H = 0$, in which H is the total Hamiltonian (7), we impose the constraint equation on the wave function of the Universe $\Psi(a, T)$,

$$\hat{H}\Psi(a, T) = 0 \ . \tag{20}$$

in which $\hat{H}$ is the Hamiltonian operator. By defining $\tau = -T$, we obtain the Wheeler-DeWitt (WdW) equation for this model,

$$-\frac{\partial^2\Psi(a,\tau)}{\partial a^2} + 2m\left(\frac{m\omega_k^2 a^2}{2} - \Lambda a^4\right)\Psi(a,\tau) = i\ 2m\frac{\partial\Psi(a,\tau)}{\partial\tau}. \tag{21}$$

We have computed the solution $\Psi(a, \tau)$ of the WdW equation numerically using finite differences in the Crank-Nicolson scheme. For details, the reader is referred to the appendix C

Here we consider wave functions that satisfy the boundary conditions established by Hartle–Hawking [47],

$$\Psi(0, \tau) = \Psi(\infty, \tau) = 0. \tag{22}$$

As $a \to \infty$, the potential becomes negligible and the wave function tends to a combination of "free" waves. The imposition that $\Psi(a \to \infty, t) = 0$ selects a physically acceptable (normalizable) solution, in which the transmitted packet disperses and its local probability density decays in time and space, characterizing an open scattering problem with unidirectional probability flux. If this asymptotic condition were not imposed, the problem would no longer be well-posed in the spectral sense of the Hamiltonian operator and, from a numerical point of view, it would be equivalent to solving the evolution equation on a finite domain with reflective boundary conditions. In this scenario, the transmitted component would *not* be absorbed at infinity but would be reflected at the boundary a_{max}, returning to the barrier region. This would introduce additional terms in the probability flux (which can be interpreted as multiple successive incidences on the barrier, analogous to a geometric series of reflections). Consequently, the probability density exhibits stationary interference patterns; the local norm would no longer represent a simple flux scattering, and the calculated tunneling probability would become dependent on the simulation time. Formally, the system would no longer be an open-domain scattering problem; rather, it would become an eigenvalue problem in a "box", with a discretized spectrum and dynamics dominated by artificial reflections, thus compromising the physical interpretation of the results.

For a discussion on the self-adjointness of the Hamiltonian operator the boundary conditions (22), the reader is referred to the Appendix D.

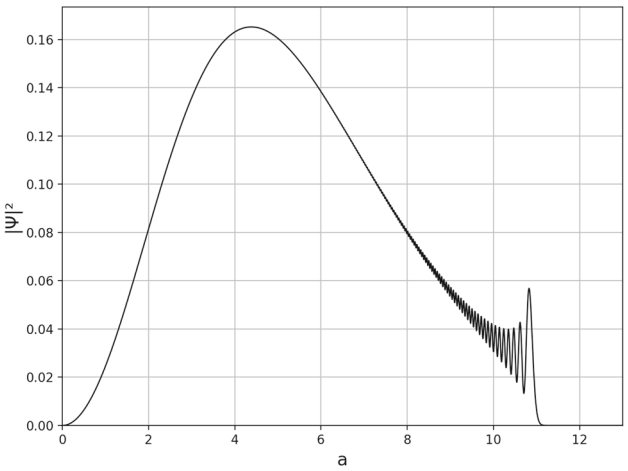

Fig. 8 Probability Density $|\Psi(a, \tau_{max})|^2$ for the fluid energy $\overline{E} = 179.8$

3.2 Integrated tunneling probability ($T\,P_{int}$)

The tunneling probability can also be calculated as the odds for the Universe to be found at the right side of the potential barrier. Therefore, we define the *integrated tunneling probability* [48,49] as

$$T\,P_{int} = \frac{\int_{a_{rtp}}^{\infty} |\Psi(a, \tau_{max})|^2 da}{\int_0^{\infty} |\Psi(a, \tau_{max})|^2 da}, \tag{23}$$

in which the infinite upper limit of integration is, in practice, replaced by a suitably large numerical value (the *numerical infinity*).

We chose the initial condition as [50]

$$\psi(a) \equiv \Psi(a, 0) = 2.481612957\left(\frac{m^3\overline{E}^3}{\pi}\right)^{\frac{1}{4}} a\, e^{-\frac{2}{3}m\overline{E}a^2}, \tag{24}$$

which automatically satisfies the boundary conditions (22). Here, $\overline{E}$ represents the radiation fluid's energy. Figure 8 shows the probability density $|\Psi(a, \tau_{max})|^2$, in which τ_{max} is the moment when the wave function reaches the numerical infinity.

3.3 Expectation values in the many worlds interpretation

Proposed by Hugh Everett III, the main statement of the *Many-Worlds* (MW) interpretation of Quantum Mechanics [51,52] is that the wave function of the Universe is made up of quantum superpositons. In this framework there is no collapse of the wave function, as it happens in the Copenhagen interpretation. That interpretation fits accordingly in the context of quantum cosmology models being described

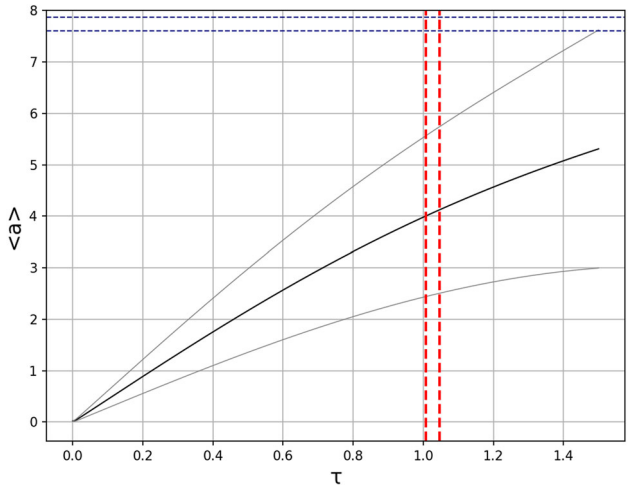

Fig. 9 Expectation value $\langle a(\tau)\rangle$ (black line) and $\langle a(\tau)\rangle \pm \varepsilon(\tau)$ (grey lines). The horizontal dashed lines near the top are the values of the scale factor a_{ltp} and a_{rtp}, corresponding to the classical left and right turning points, respectively. The two vertical lines indicate τ_l and τ_r, the values of τ at which the wave hits those turning points

by the Wheeler-DeWitt equation (21). This equation is independent of an external time parameter, suggesting that the classical notion of temporal evolution emerges only locally within each element of the wave function quantum superposition. In the MW interpretation the scale factor's behavior may be studied through the analysis of its expectation value given by

$$\langle a(\tau)\rangle = \frac{\int_0^\infty \Psi^\star(a,\tau)\, a\, \Psi(a,\tau) da}{\int_0^\infty \Psi^\star(a,\tau)\, \Psi(a,\tau) da}. \tag{25}$$

Using the initial condition (24) we have solved the Wheeler-DeWitt equation (21) numerically for $\Psi(a,\tau)$, and then evaluated the expectation value $\langle a(\tau)\rangle$ in (25). We let $\Lambda = 0.05, \beta = 0.27$ and $\sigma = 0.9999$ for the model parameters mentioned in Eq. (9); the number of space points $N_s = 20,000$ and τ points $N_\tau = 1000$ for the numerical grid; and the steps $da = 0.003$ and $d\tau = 0.0015$, for the spatial and fluid variables, respectively. The result is represented by the central black line in Fig. 9; the adjacent grey lines correspond to $\langle a(\tau)\rangle \pm \varepsilon(\tau)$, in which $\varepsilon(\tau)$ is the standard deviation

$$\varepsilon(\tau) = \sqrt{\langle a(\tau)^2\rangle - \langle a(\tau)\rangle^2}. \tag{26}$$

3.4 On the inflationary behavior in the quantum model

The birth of the classical Universe is set as the quantum wave reaches the right turning point of the potential barrier a_{rtp}, at $\tau = \tau_{rtp}$. For $\tau > \tau_{rtp}$, we expect cosmic inflation to take place. The expectation value of the scale factor becomes

$$\langle a_{pb}(\tau)\rangle = \frac{\int_{a_{rtp}}^\infty \Psi^\star(a,\tau) a \Psi(a,\tau) da}{\int_{a_{rtp}}^\infty \Psi^\star(a,\tau)\Psi(a,\tau) da}, \tag{27}$$

in which pb stands for "post barrier".
The behavior of $\langle a_{pb}(\tau)\rangle$ shown in Fig. 10a and b depict the same curve, but in normal and logarithmic scale, respectively. We let $E = 179.8$; at $\tau_{initial} \equiv \tau_{rtp} = 1.4125$ the wave function hits the right side of the barrier (i.e., the onset of the classical Universe) and then the scale factor shows accentuated exponential growth; we found that at $\tau_{final} = 1.1300 \times 10^{10}$, in the quantum model (which we emphasize because the variables τ and η are not the same), we obtain $\langle a_{pb}(\tau_{initial})\rangle = 7.999643$ and $\langle a_{pb}(\tau_{final})\rangle = 1.618687 \times 10^{27}$, yielding and expansion ratio of 2.023449×10^{26}.

4 Dependence of tunneling probabilities on the parameters of the theory

In this section, we compare the tunneling probability in the WKB approximation TP_{WKB} (150) with the integral tunneling probability TP_{int} (23), regarding their dependence on the energy $\overline{E}$ and on (Λ, σ, β). Calculations related to the WKB approximation can be found in Appendix E

4.1 Tunnelling probabilities dependence on the Energy E

By fixing $\sigma = 0.9999$, $\beta = 0.27$, $k = 1$, $\Lambda = 0.05$ and $\omega = 1/3$ for radiation, the maximum value of the potential (8) is $V_{max} = 180.035845$. So we varied the energy $E \in [1,5]$ in steps $\Delta E = 1$; $\overline{E} \in [10,170]$ in steps $\Delta E = 10$, and then chose two final values, $\overline{E} = 175$ and $\overline{E} = 179.8$, near the top of the potential barrier. Figure 11 compares the tunneling probabilities TP_{int} and TP_{WKB}, which differ for lower values of energy but converge as the energy reaches the top of the barrier.

Near the top of the barrier, the agreement between TP_{int} and TP_{WKB} can be understood from the effective dynamics of the wave packet in this regime. For average energies $\overline{E}$ close to the maximum value of the potential, the barrier becomes relatively narrow and low, which reduces the typical exponential damping of tunneling. In this situation, the assumptions underlying the validity of the WKB approximation are better satisfied, as the potential varies more smoothly in the classically forbidden region. In addition, the time required for the reflected component of the packet to return to the interaction region (once gone through the barrier and reflected by the infinite wall at $a = 0$) becomes sufficiently large. Thus, during the time interval considered in the numerical calculation, the dynamics are essentially dominated by a single-incidence process on the barrier, which is the scenario described by the WKB approximation.

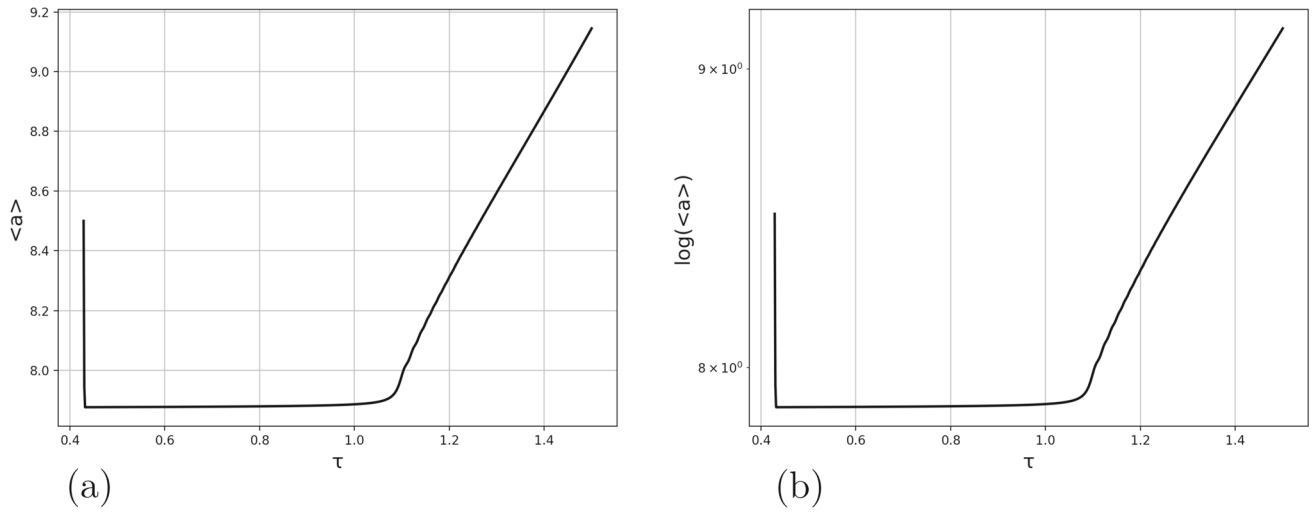

Fig. 10 Expectation values $< a_{pb}(\tau) >$, for $a > a_{rtp}$. Panels (**a**) and (**b**) depict the same curve, in normal and logarithmic scale, respectively. Right after the wave function reaches the right turning point a_{rtp} at $\tau_{initial} = 1.4125$, it exhibits exponential growth

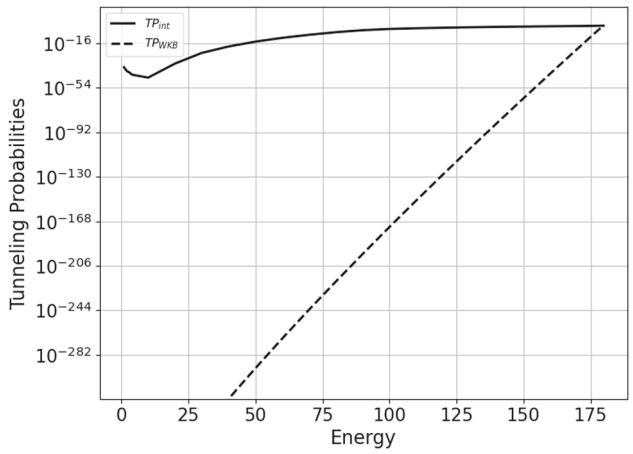

Fig. 11 Comparison between TP_{int} (solid line) and TP_{WKB} (dashed line) as the energy $\overline{E}$ varies. We let $\sigma = 0.9999$, $\beta = 0.27$, $k = 1$, $\Lambda = 0.05$ and $\omega = 1/3$. Both converge to same value, as the energy approaches the top of the potential barrier

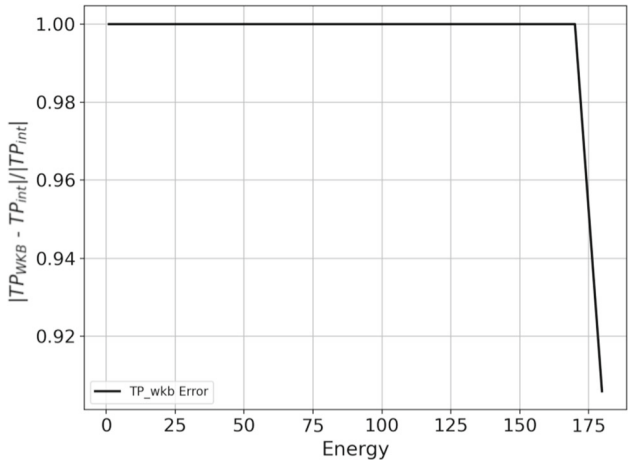

Fig. 12 Relative error between TP_{int} and TP_{WKB}. We have used $N = 20{,}000$, $X_{max} = 60$, $t_{max} = 1.5$, $dt = 0.015$ for the initial condition (24)

On the other hand, for average energies $\overline{E}$ much lower than that of the top of the barrier, the system behaves qualitatively different. In this case, the effective barrier is wider and higher, making the transmission probability predicted by the WKB approximation extremely small, due to the strong exponential damping factor. The presence of an infinite potential wall at $a = 0$, however, prevents the reflected component from dissipating, as it would in a usual scattering problem. Instead, the reflected wave returns and reaches the barrier again, generating successive tunneling events. Each of these incidences contributes a small fraction of transmitted probability, and the cumulative effect of these multiple reflections can be interpreted as a sum of contributions analogous to a geometric series. Since the reflection coefficient is close to unity in this regime, such accumulation becomes significant, leading to a total tunneling probability much larger than the one predicted by the WKB approximation, which considers only a single incidence.

Hence the difference between the two results is directly associated with the effective open or confined nature of the system. Near the top of the barrier, the problem behaves like an open-domain scattering scenario, where the WKB approximation is appropriate. For low energies, however, the system behaves like a quantum cavity, in which multiple reflections amplify the transmission probability, rendering the WKB estimate insufficient to correctly describe the tunneling process (Fig. 12).

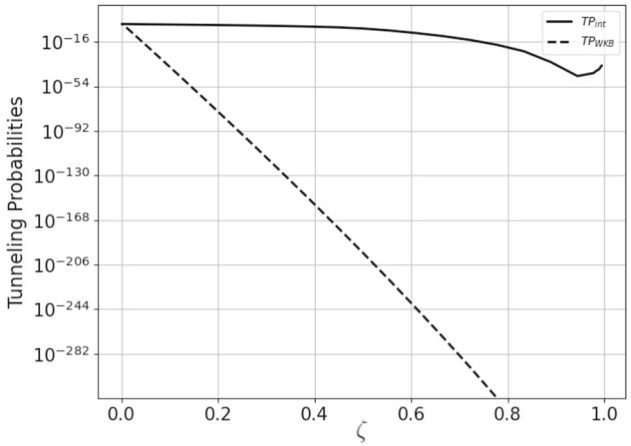

Fig. 13 Comparison of tunneling probabilities TP_{int} (Crank-Nicolson) and TP_{WKB} (WKB method), calculated for the initial condition $\psi^{(1)}(a)$, in the adimensional variable $\zeta = 1 - \overline{E}/V_{max}$

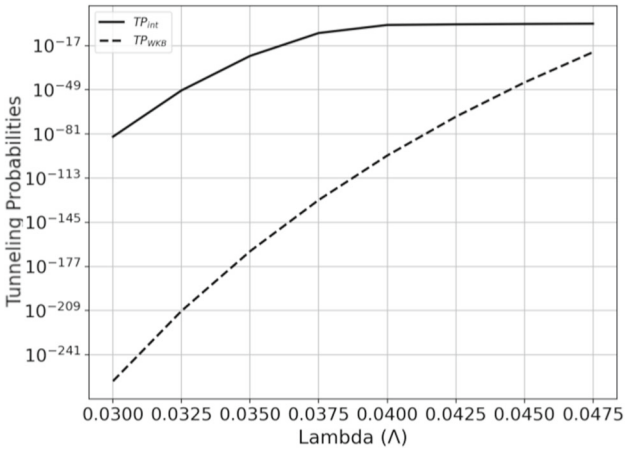

Fig. 14 Comparison between TP_{int} (solid line) and TP_{WKB} (dashed line) as the cosmological constant Λ varies. We let $\sigma = 0.9999$, $\beta = 0.27$, $k = 1$, $\omega = 1/3$ and $E = 179$. Both approach the same value, as Λ increases

The effective potential, defined in Eq. (8) can be rewritten in terms of the constants Λ, k, β and σ as

$$V(a) = \frac{6k}{\sigma}a^2 - \Lambda a^4. \tag{28}$$

This potential reaches its maximum value at $a = a_m$, so that

$$\left.\frac{dV(a)}{da}\right|_{a=a_m} = 0 \quad \longrightarrow \quad a_m = \sqrt{\frac{3k}{\Lambda\sigma}}, \tag{29}$$

which is

$$V_{max} = V(a_m) = \frac{9k^2}{\Lambda\sigma^2} \tag{30}$$

Reploting the dependency of the tunneling probabilities TP_{int} (Crank-Nicolson) and TP_{WKB} in terms of the adimensional variable $\zeta = 1 - \dfrac{\overline{E}}{V_{max}}$, we obtain Fig. 13.

4.2 Tunnelling probabilities dependence on the cosmological constant Λ

By fixing $\sigma = 0.9999$, $\beta = 0.27$, $k = 1$, $\omega = 1/3$ and $E = 179$ and varying $\Lambda \in [0.03, 0.05]$ in steps of $\Delta\Lambda = 0.0025$, we have obtained Fig. 14, which exemplifies the behavior of the tunneling probabilities: as Λ increases, both TP_{int} and TP_{WKB} increase and converge to the same value. The maximum value of the potential decreases as Λ increases; the value of E has been chosen by taking into account that variation, $V_{max}(\Lambda) \in [180.035845, 300.060006]$ in the interval of Λ under consideration.

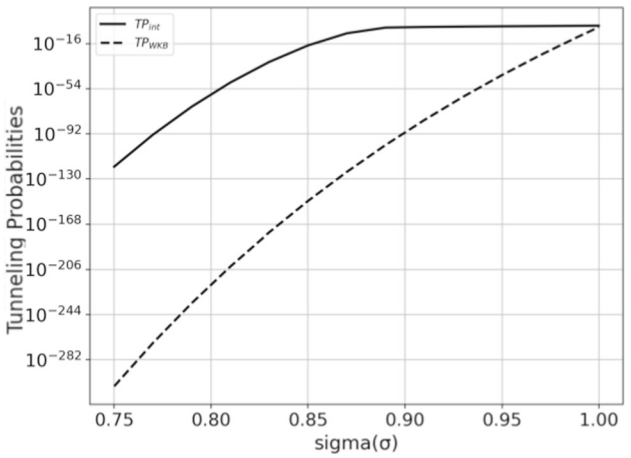

Fig. 15 Comparison between TP_{int} (solid line) and TP_{WKB} (dashed line) as σ varies. We let $\beta = 0.27$, $k = 1$, $\Lambda = 0.05$, $\omega = 1/3$ and $E = 179$. Both approach the same value, as σ increases

4.3 Tunnelling Probabilities dependence on the Einstein–Aether parameter σ

By fixing $\beta = 0.27$, $k = 1$, $\Lambda = 0.05$ and $\omega = 1/3$ and $E = 179$ and varying $\sigma \in [0.75, 0.99]$ in steps $\Delta\sigma = 0.02$, we have obtained Fig. 15. As σ increases, both tunneling probabilities TP_{int} and TP_{WKB} increase, and converge to the same value. The value of E, once more, has been chosen by taking into account the variation of the top of the barrier, which decreases in the interval of σ under consideration and $V_{max}(\sigma) \in [180.035845, 319.99947]$.

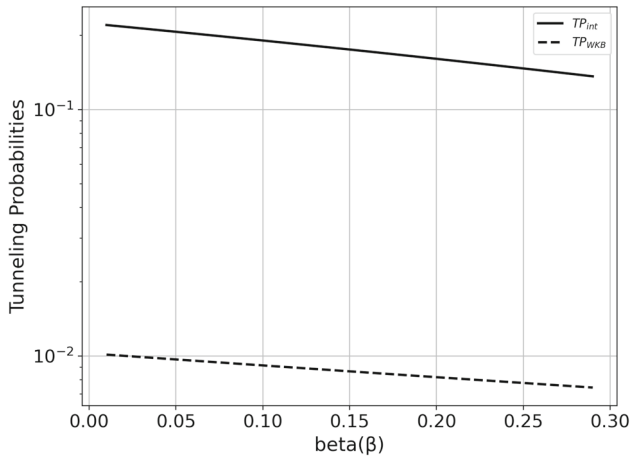

Fig. 16 Comparison between TP_{int} and TP_{WKB} using $\sigma = 0.9999$, $k = 1$, $\Lambda = 0.05$, $\omega = 1/3$ and $E = 179$

4.4 Tunnelling probabilities dependence on the Einstein–Aether parameter β

In order to investigate the behavior of the tunneling probabilities as one varies the β parameter, it was set that $\sigma = 0.9999$, $k = 1$, $\Lambda = 0.05$ and $\omega = 1/3$. The β parameter was chosen to vary within a range that goes from $\beta = 0.01$ to $\beta = 0.3$ in steps of 0.01. Once again, a fixed energy value was chosen taking in consideration the maximum values of the potential calculated using the minimum and maximum values of β in the interval we chose. Since $V_{max}(\beta = 0.01) = 180.03584579161030$ and $V_{max}(\beta = 0.3) = 180.03584579161037$, it was decided that $E = 179$. As one can see in Fig. (16), as beta grows, the value of the tunneling probabilities diminishes. This means that a smaller value of β implies a higher tunneling probability.

4.5 Tunneling probabilities and the quantum initial state

In Sect. 3.2 we used the quantum initial condition (24), which we will rename here as

$$\psi_0^{(1)}(a) = 2.481612957 \left(\frac{m^3\overline{E}^3}{\pi}\right)^{\frac{1}{4}} a\, e^{-\frac{2}{3}m\overline{E}a^2}. \tag{31}$$

In this subsection we examine the behavior of the integrated tunneling probabilities TP_{int} for two other initial conditions,

$$\psi_0^{(2)}(a) = \sqrt{1.472970576}\,(m\overline{E})^{5/4}\, a^2 \exp\left(-0.3068688699\,(m\overline{E})^{3/2}\, a^3\right), \tag{32}$$

and

$$\psi_0^{(3)}(a) = \sqrt{4m\overline{E}}\; a\; \exp\left(-\frac{2}{3}m\overline{E}\, a^3\right). \tag{33}$$

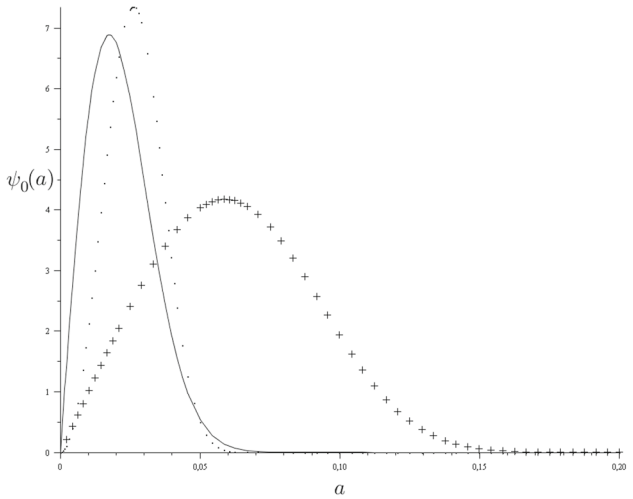

Fig. 17 Several initial conditions. $\psi_0^{(1)}(a)$ (solid line) is the one used in the manuscript. $\psi_0^{(2)}(a)$ (dotted line) and $\psi_0^{(3)}(a)$ (cross line) are slightly different initial conditions, used here for the sake of comparison among the corresponding tunneling probabilities

These three conditions are simultaneously represented in Fig. 17. The initial condition $\psi_0^{(2)}(a)$ is slightly more localized than the original $\psi_0^{(1)}(a)$, whereas $\psi_0^{(3)}(a)$ spreads over a slightly larger interval than $\psi_0^{(1)}(a)$.

The deviation from unity norm of the wave functions evolved from all three initial states were numerically calculated at various time instants, being of order 10^{-13} in magnitude.

For the initial condition (31), the tunneling probabilities as a function of energy $\overline{E}$ are shown in Fig. 11. For the initial conditions (32) and (33), in the same range of energies, the tunneling probabilities are represented in Fig. 18.

5 Discussion and conclusions

We studied a FLRW cosmological model within the framework of Einstein–Aether gravity, with positive spatial curvature and matter content described by a radiation perfect fluid and dark energy, the latter being represented by a cosmological constant term Λ. The classical phase space of the model was constructed. We then obtained a differential equation for the scale factor that confirms the types of solutions identified in the phase-space analysis.

Subsequently, we demonstrated that specific initial conditions in regions II and III of the (a, p_a) plane of the phase space lead to an inflationary expansion after the Universe emerges from the quantum phase. This behavior is corroborated by the evolution of both the Hubble parameter H_b and the deceleration parameter q.

Proceeding to the quantum description, we applied the Dirac formalism to quantize the model. The resulting Wheeler-DeWitt equation was solved both numerically and

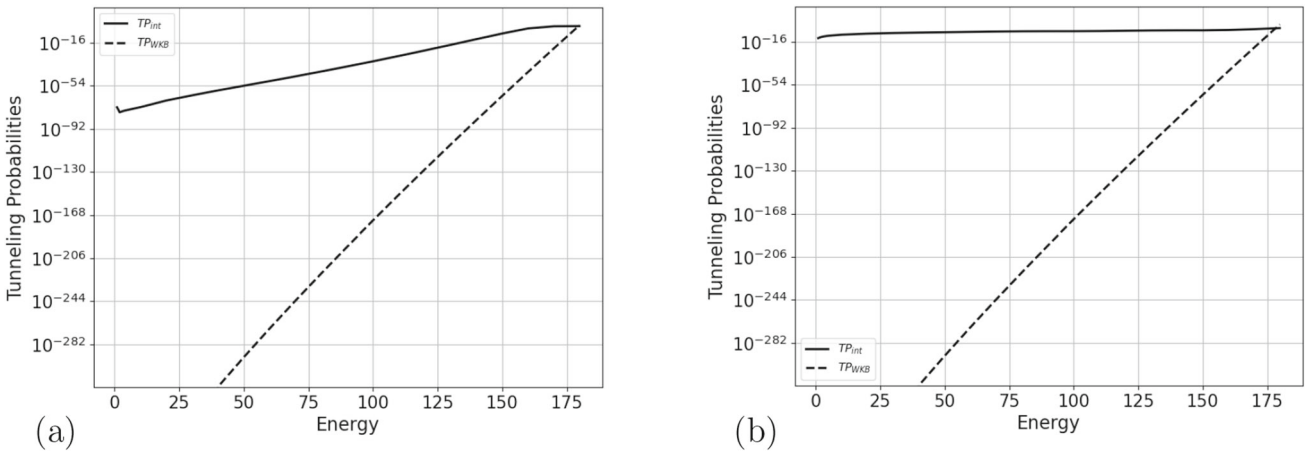

Fig. 18 Tunneling probabilities numerically calculated (solid lines) for the initial conditions **a** $\psi_0^{(2)}$ and **b** $\psi_0^{(3)}$. The dashed lines correspond to tunneling probabilities based on the WKB approximation

via the WKB approximation. These solutions enabled the computation of quantum tunneling probabilities and the expectation values for the scale factor $\langle a \rangle$, along with its corresponding standard deviations ε.

We systematically calculated the influence of each model parameter and the fluid energy E on the tunneling probabilities $T P_{\text{int}}$ and $T P_{\text{WKB}}$. Our results indicate that increasing the cosmological constant Λ, the parameter σ, or the energy E leads to higher tunneling probabilities. At the same time, higher values of β implies on lower tunnelling probabilities values. Therefore, we conclude that for this model, the quantum birth of the Universe is more probable with higher values of Λ, σ and E and lower values of β.

Acknowledgements G. A. Monerat thanks FAPERJ for partial financial support. G.A. Monerat and E. V. Corrêa Silva thanks Universidade do Estado do Rio de Janeiro, UERJ, for the Prociência grant. A. Oliveira Castro Júnior thanks CAPES for financial support. This study was financed in part by the Coordenação de Aperfeiçoamento de Pessoal de Nível Superior ¨ Brasil (CAPES)¨ Finance Code 001. G. Oliveira-Neto thanks FAPEMIG (APQ-06640-24) for partial financial support.

Author contributions All authors contributed to every stage of the paper, including the writing.

Funding not applicable in our research shown here.

Data availability statement This manuscript has no associated data. [Author's comment: Data sharing not applicable to this article as no datasets were generated or analysed during the current study.]

Code availability statement This manuscript has no associated code/software. [Author's comment: Code/Software sharing not applicable to this article as no code/software was generated or analysed during the current study.]

Declarations

Conflict of interest not applicable in our research shown here.
Ethical approval not applicable in our research shown here.

Funded by SCOAP[3].

A The Hamiltonian of the Einstein–Aether model

The total action of Einstein–Aether theory consists of three fundamental contributions,

$$\mathcal{S} = S_{EH} + S_{EA} + S_{matter}, \tag{34}$$

in which S_{EH} is the Einstein-Hilbert action of General Relativity, S_{EA} contains the dynamics of the aether vector field, and S_{matter} describes the conventional matter fields, minimally coupled to the metric.

The action of the aether sector [53] with $c = 1$ is

$$S_{AE} = \frac{1}{16\pi G}\int d^4x\sqrt{-g}\left[-K^{\alpha\beta}_{\mu\nu}\nabla_\alpha u^\mu \nabla_\beta u^\nu + \lambda\left(g_{\mu\nu}u^\mu u^\nu + 1\right)\right] \tag{35}$$

in which g is the determinant of the metric, λ is the Lagrange multiplier ensuring that the field u^μ is always unitary and timelike, ∇_α denotes the covariant derivative, and u^μ is the aether field, a dynamical timelike vector field defined

throughout spacetime. The coupling tensor $K^{\alpha\beta}_{\mu\nu}$ is

$$K^{\alpha\beta}_{\mu\nu} = c_1\, g^{\alpha\beta} g_{\mu\nu} + c_2\, \delta^{\alpha}_{\mu}\delta^{\beta}_{\nu} + c_3\, \delta^{\alpha}_{\nu}\delta^{\beta}_{\mu} - c_4\, u_{\alpha}u_{\beta}g_{\mu\nu}. \quad (36)$$

Our interest lies in homogeneous and isotropic models. Thus, we consider the Friedmann-Robertson-Walker metric in cosmological time, with the lapse function $N = 1$

$$ds^2 = -dt^2 + a(t)^2\left[\frac{dr^2}{1-kr^2} + r^2\left(d\theta^2 + \sin^2(\theta)d\phi^2\right)\right], \quad (37)$$

in which $a(t)$ is the scale factor, k is the curvature of the spatial section, such that $k = -1$ for open, $k = 0$ for flat, and $k = 1$ for closed Universes.

For homogeneous and isotropic universes, the most general form of the aether field compatible with the symmetries is

$$u^{\alpha} = (1,\, 0,\, 0,\, 0)\,, \quad u_{\alpha} = (-1,\, 0,\, 0,\, 0)\,, \quad (38)$$

so that the field u^{α} is a unit timelike vector satisfying the normalization condition

$$u^{\alpha}u_{\alpha} = -1. \quad (39)$$

According to (35), the aether Lagrangian is

$$\mathcal{L}_{EA} = -\frac{\sqrt{-g}}{16\pi G}\left[K^{\alpha\beta}_{\mu\nu}\nabla_{\alpha}u^{\mu}\nabla_{\beta}u^{\nu} + \lambda\left(g_{\mu\nu}u^{\mu}u^{\nu} + 1\right)\right] \quad (40)$$

From (39), we get $g_{\mu\nu}u^{\mu}u^{\nu} = -1$; thus the term with λ vanishes. Then

$$\mathcal{L}_{EA} = -\frac{\sqrt{-g}}{16\pi G}\left[K^{\alpha\beta}_{\mu\nu}\nabla_{\alpha}u^{\mu}\nabla_{\beta}u^{\nu}\right] \quad (41)$$

with $K^{\alpha\beta}_{\mu\nu}$ given by (36).

The covariant derivative of the field u_{ν} is

$$\nabla_{\mu}u_{\nu} = \partial_{\mu}u_{\nu} - \Gamma^{\lambda}_{\mu\nu}u_{\lambda}. \quad (42)$$

Since $u_{\nu} = (-1,\, 0,\, 0,\, 0)$

$$\partial_{\mu}u_{\nu} = 0. \quad (43)$$

So,

$$\nabla_{\mu}u_{\nu} = -\Gamma^{\lambda}_{\mu\nu}u_{\lambda}. \quad (44)$$

Since $u_i = 0$ and $u_0 = -1$, we have

$$\nabla_{\mu}u_{\nu} = \Gamma^{0}_{\mu\nu}. \quad (45)$$

Now we need to compute the Christoffel symbols for the FRW metric. The vanishing covariant components of the metric are

$$g^{\mu\alpha}g_{\alpha\nu} = \delta^{\mu}_{\nu}, \quad (46)$$

recalling that $g^{\mu\nu}$ is the inverse of $g_{\mu\nu}$. Then, the non-vanishing components of the covariant form of the metric are

$$g_{00} = -1,\; g_{11} = \frac{a^2}{1-kr^2},\; g_{22} = a^2r^2,\; g_{33} = a^2r^2\sin^2\theta,$$
$$g_{0l} = 0, \quad \forall\, l \in \{1, 2, 3\}. \quad (47)$$

keeping in mind that $a = a(t)$. In their turn, the non-vanishing components of the contravariant form of the metric are

$$g_{00} = -1,\; g_{11} = \frac{1-kr^2}{a^2},\; g_{22} = \frac{1}{a^2r^2},\; g_{33} = \frac{1}{a^2r^2\sin^2\theta},$$
$$g_{0l} = 0, \quad \forall\, l \in \{1, 2, 3\}. \quad (48)$$

The Christoffel symbols are defined as

$$\Gamma^{\alpha}_{\mu\nu} = \frac{1}{2}g^{\alpha\sigma}\left(\partial_{\mu}g_{\nu\sigma} + \partial_{\nu}g_{\mu\sigma} - \partial_{\sigma}g_{\mu\nu}\right). \quad (49)$$

By expanding the sum over σ in expression (49) we obtain

$$\Gamma^{0}_{00} = 0, \quad \Gamma^{0}_{ij} = a\dot{a}\gamma_{ij}, \quad \Gamma^{i}_{0j} = \frac{\dot{a}}{a}\delta^{i}_{j}, \quad (50)$$

in which $g^{il} = \frac{\gamma^{il}}{a^2}$.

A.1 The components $\nabla_{\alpha}u^{\mu}$

We have

$$\nabla_{\alpha}u^{\mu} = \Gamma^{\mu}_{0\alpha} \quad (51)$$

then

$$K^{\alpha\beta}_{\mu\nu}\nabla_{\alpha}u^{\mu}\nabla_{\beta}u^{\nu} = K^{\alpha\beta}_{\mu\nu}\Gamma^{\mu}_{0\alpha}\Gamma^{\nu}_{0\beta}. \quad (52)$$

According to (36) $K^{\alpha\beta}_{\mu\nu}$ has four terms, so we will calculate each one of them separately:

$$c_1 g^{\alpha\beta}g_{\mu\nu}\Gamma^{\mu}_{0\alpha}\Gamma^{\nu}_{0\beta} = 3c_1\left(\frac{\dot{a}}{a}\right)^2, \quad (53)$$

$$c_2\delta^{\alpha}_{\mu}\delta^{\beta}_{\nu} = 9c_2\left(\frac{\dot{a}}{a}\right)^2, \quad (54)$$

$$c_3\delta^{\alpha}_{\nu}\delta^{\beta}_{\mu}\Gamma^{\mu}_{0\alpha}\Gamma^{\nu}_{0\beta} = 3c_2\left(\frac{\dot{a}}{a}\right)^2, \quad (55)$$

$$c_4 u^\alpha u^\beta g_{\mu\nu}\Gamma^\mu_{0\alpha}\Gamma^\nu_{0\beta} = 0. \tag{56}$$

According to these results and knowing that $\sqrt{-g} \sim a^3$, the Einstein-aether Lagrangian takes the form

$$\mathcal{L}_{EA} = -\frac{-3(c_1 + 3c_2 + c_3)}{16\pi G} a\dot{a}^2. \tag{57}$$

In Einstein–Aether theory,

$$G = \sigma\ G_N \tag{58}$$

in which

$$\sigma = 1 - \frac{c_1 + c_4}{2} \tag{59}$$

and G_N is Newton's gravitational constant. Here we will set $16\pi G_N = 1$, thus

$$\mathcal{L}_{EA} = -\frac{3\beta}{\sigma} a\dot{a}^2. \tag{60}$$

in which

$$\beta = c_1 + 3c_2 + c_3 \tag{61}$$

A.2 The Einstein–Hilbert action

Considering now the Einstein–Hilbert action

$$S_{EH} = \frac{1}{\sigma}\int_{\mathcal{M}} d^4x\sqrt{-g}R, \tag{62}$$

in which σ is defined in Eq. (9). The Ricci curvature scalar takes the form

$$R = \frac{\ddot{a}}{a} + \frac{\dot{a}^2}{a^2} + \frac{k}{a^2}, \tag{63}$$

so that we can write (62) as

$$S_{EH} \propto \frac{1}{\sigma}\int dt a^3 R \tag{64}$$

or

$$S_{EH} \propto \frac{1}{\sigma}\int 6\left(a^2\ddot{a} + a\dot{a}^2 + ka\right) dt \tag{65}$$

Then, the Einstein–Hilbert Lagrangian takes the form

$$\mathcal{L}_{EH} = \frac{6}{\sigma}\left(a^2\ddot{a} + a\dot{a}^2 + ka\right). \tag{66}$$

The second derivative term in the Lagrangian can be eliminated by the extraction of a total time derivative,

$$a^2\ddot{a} = \frac{d}{dt}\left(a^2\dot{a} - 2a\dot{a}^2\right), \tag{67}$$

Then

$$\mathcal{L}_{EH} = \frac{6}{\sigma}\left(-a\dot{a}^2 + ka\right). \tag{68}$$

The Lagrangian of the gravitational sector $\mathcal{L}_G$ will be the sum of the Lagrangians (61) and (68),

$$\mathcal{L}_G = -\frac{3(\beta+2)}{\sigma} a\dot{a}^2 + \frac{6k}{\sigma} a. \tag{69}$$

A.3 The matter action

In order to include the material content of the Universe, we use the Schultz formalism, in which matter is represented by a perfect barotropic fluid. In this case, the matter action is given by

$$\mathcal{S}_m = \int_M d^4x\ \sqrt{-g}\ p \tag{70}$$

and the covariant four-velocity is written as

$$u_\nu = \left(\frac{1}{\mu}\left[\partial_\nu\epsilon + \theta\ \partial_\nu S + \chi\ \partial_\nu\Xi\right],\ 0,\ 0,\ 0\right), \tag{71}$$

in which μ is the specific enthalpy, S is the specific entropy, and ϵ, θ, Ξ, and χ are scalar potentials of the fluid. The terms Ξ and χ describe rotational degrees of freedom (vorticity) of the fluid. Homogeneous and isotropic models have no vorticity, though; hence,

$$\chi\ \partial_\nu\Xi = 0, \tag{72}$$

and

$$u_\nu = \left(\frac{1}{\mu}\left[\partial_\nu\epsilon + \theta\ \partial_\nu S\right],\ 0,\ 0,\ 0\right). \tag{73}$$

In cosmologies with the FLRW metric, it is assumed that the fluid is at rest in comoving coordinates,

$$u_\mu = (-1,\ 0,\ 0,\ 0). \tag{74}$$

From the relation $u^\mu u_\mu = -1 \rightarrow u^0 u_0 = -1 \rightarrow g^{00}u_0^2 = -1$ we then have

$$\mu = \partial_\nu\epsilon + \theta\partial_\nu S. \tag{75}$$

From (73),

$$\partial_\nu\epsilon = (\dot{\epsilon},\ 0,\ 0,\ 0) \tag{76}$$

and

$$\partial_\nu S = \left(\dot{S},\ 0,\ 0,\ 0\right). \tag{77}$$

Substituting (76) and (77) into (73) we obtain

$$u_v = \frac{1}{\mu}(\dot{\epsilon} + \theta \dot{S})\,. \tag{78}$$

and

$$\mu = \dot{\epsilon} + \theta \dot{S}. \tag{79}$$

We now use the first law of thermodynamics,

$$d\rho = \mu\, dn + nT\, dS, \tag{80}$$

in which ρ is the internal energy density of the fluid, n is the particle number, T is the temperature, S is the specific entropy, and μ is the specific enthalpy of the fluid.

The specific enthalpy can also be written as

$$\mu = \frac{\rho + p}{n}. \tag{81}$$

In our model we are considering a barotropic fluid $p = \alpha\rho$, so that (81) becomes

$$\mu = \frac{(1+\alpha)\rho}{n} \rightarrow \rho = \frac{n\mu}{(1+\alpha)}. \tag{82}$$

Substituting (82) into (80), we get

$$d\rho = \frac{(1+\alpha)}{n}\rho\, dn + nT\, dS. \tag{83}$$

or

$$\frac{d\rho}{\rho} = \frac{(1+\alpha)}{n} dn + \frac{nT}{\rho} dS. \tag{84}$$

Integrating, one obtains

$$\rho = C_0 \cdot n^{1+\alpha} \cdot e^{\int f(S) dS}, \tag{85}$$

in which

$$f(S) = \frac{nT}{\rho}. \tag{86}$$

From (81),

$$\mu = \left(\frac{\partial \rho}{\partial n}\right)_S = \frac{(1+\alpha)}{n}\rho \tag{87}$$

So,

$$\frac{\partial \rho}{\partial n} = \frac{(1+\alpha)}{n}\rho \rightarrow \frac{1}{\rho}\partial\rho = \frac{(1+\alpha)}{n}\partial n. \tag{88}$$

Integrating, we get

$$\rho = n^{1+\alpha} h(S). \tag{89}$$

Comparing (85) and (89),

$$h(S) = C_0 e^{\int f(S) dS}. \tag{90}$$

Consequently,

$$\frac{d}{dS}h(S) = C_0 e^{\int f(S) dS} \cdot \frac{d}{dS}\int f(S) dS = h(S) \cdot f(S). \tag{91}$$

Then

$$f(S) = \frac{\frac{dh(S)}{dS}}{h(S)} \tag{92}$$

The relation to the temperature T comes from

$$T = \frac{1}{n}\left(\frac{\partial \rho}{\partial S}\right)_n \tag{93}$$

By using (89) in (93) we get

$$T = n^{\alpha}\frac{dh(S)}{dS} \tag{94}$$

and

$$\mu = (1+\alpha) n^{\alpha} h(S). \tag{95}$$

Isolating n,

$$n = \left(\frac{\mu}{(1+\alpha)h(S)}\cdot\right)^{1/\alpha} \tag{96}$$

Substituting (96) into (89),

$$\rho = (1+\alpha)^{-\left(\frac{1+\alpha}{\alpha}\right)} \mu^{\left(\frac{1+\alpha}{\alpha}\right)} h(S)^{-\frac{1}{\alpha}}. \tag{97}$$

Using now the equation of state $p = \alpha\rho$, we have

$$p = \alpha \left(\frac{\mu}{(1+\alpha)}\right)^{\frac{1+\alpha}{\alpha}} h(S)^{-\frac{1}{\alpha}}. \tag{98}$$

The function $h(S)$ is determined by the choice of variable for the entropy. Equation (89) yields

$$h(S) = e^{S}, \tag{99}$$

without loss of generality.

$$p = \alpha \left(\frac{\mu}{(1+\alpha)}\right)^{\frac{1+\alpha}{\alpha}} e^{-\frac{S}{\alpha}}. \tag{100}$$

Substituting (79) into (100),

$$p = \alpha \left(\frac{\dot{\epsilon} + \theta \dot{S}}{1+\alpha} \right)^{\frac{1+\alpha}{\alpha}} e^{-\frac{S}{\alpha}}. \tag{101}$$

The matter action

$$\mathcal{S}_m = \int d^4x \sqrt{-g}\, p, \tag{102}$$

can be expressed now as

$$\mathcal{S}_m \propto \int_t a^3 \cdot \alpha \left(\frac{\dot{\epsilon} + \theta \dot{S}}{1+\alpha} \right)^{\frac{1+\alpha}{\alpha}} e^{-\frac{S}{\alpha}} dt. \tag{103}$$

Hence, the matter lagrangian gets the form

$$\mathcal{L}_m = a^3 \cdot \alpha \left(\frac{\dot{\epsilon} + \theta \dot{S}}{1+\alpha} \right)^{\frac{1+\alpha}{\alpha}} e^{-\frac{S}{\alpha}}. \tag{104}$$

and the hamiltonian becomes

$$\mathcal{H}_m = \dot{\epsilon} p_\epsilon + \dot{S} p_S + \dot{\theta} p_\theta - \mathcal{L}_m. \tag{105}$$

The relation the between canonical momenta and their respective generalized coordinates is

$$p_\epsilon = \frac{\partial \mathcal{L}_m}{\partial \dot{\epsilon}} = a^3 \left(\frac{\dot{\epsilon} + \theta \dot{S}}{1+\alpha} \right)^{1/\alpha} \cdot e^{-S/\alpha}, \tag{106}$$

$$p_S = \frac{\partial \mathcal{L}_m}{\partial \dot{S}} = p_\epsilon \theta, \tag{107}$$

$$p_\theta = \frac{\partial \mathcal{L}_m}{\partial \dot{\theta}} = 0. \tag{108}$$

Hence the matter Hamiltonian (105) takes the form

$$\mathcal{H}_m = \frac{p_\epsilon^{1+\alpha} \cdot e^S}{a^{3\alpha}}. \tag{109}$$

Considering the canonical transformation

$$T = -p_S e^{-S} p_\epsilon^{-(1+\alpha)}, \quad p_T = p_\epsilon^{(1+\alpha)} e^S, \tag{110}$$

the matter Hamiltonian for a perfect fluid then takes the form

$$\mathcal{H}_m = a^{-3\alpha} p_T. \tag{111}$$

In our model we consider two fluids: a vacuum fluid ($\alpha = -1$) and a radiation fluid ($\alpha = 1/3$), so that

$$\mathcal{H}_m = a^3 \Lambda + \frac{1}{a} p_T. \tag{112}$$

The total Hamiltonian in cosmological time ($N = 1$) is

$$\mathcal{H} = -\frac{\sigma}{12(\beta+2)a} p_a^2 - \frac{6ka}{\sigma} + \Lambda a^3 + \frac{1}{a} p_T, \tag{113}$$

whereas in conformal time ($N = a$), it becomes

$$\mathcal{H} = -\frac{\sigma}{12(\beta+2)} p_a^2 - \frac{6ka^2}{\sigma} + \Lambda a^4 + p_T. \tag{114}$$

Introducing the parameters

$$m = \frac{6(\beta+2)}{\sigma}, \quad w_k = \sqrt{\frac{2k}{\beta+2}}, \tag{115}$$

the Hamiltonian in conformal time takes the form

$$\mathcal{H} = \frac{1}{2m} p_a^2 + \frac{m w_k^2}{2} a^2 - \Lambda a^4 - p_T. \tag{116}$$

B On the coupling constants and their constraints

The parameters β e σ of the Einstein–Aether (AE) theory, mentioned in Sect. 2.1, play fundamental role in the coupling between the timelike vector field u^a and the metric, as well as in the definition of the effective gravitational constant. Their precise definitions, in terms of the adimensional coupling constants c_i (of the aether action) are

$$\beta = c_1 + 3c_2 + c_3, \tag{117}$$

$$\sigma = 1 - \frac{c_{14}}{2}, \quad \text{in which} \quad c_{14} = c_1 + c_4. \tag{118}$$

Those parameters emerge naturally as one writes the complete gravitational action in the ADM formalism and considers the Friedmann equations, modified by the aether.

In order to describe a physically meaningful model, the constants c_i are subject to a set of theoretical and observational constraints that guarantee the absence of instabilities (e.g. ghosts, tachions) an the compatibility with experimental data. The main constraints are as follows [53].

1. **Wave modes velocities** – The quadratic velocities of the five modes propagated by the theory (spin-0, spin-1 and spin-2) must be positive and real.

$$s_0^2 = \frac{c_{123}(2 - c_{14})}{c_{14}(1 - c_{13})(2 + c_{13} + 3c_2)},$$
$$s_1^2 = \frac{2c_1 - c_1^2 + c_3^2}{2c_{14}(1 - c_{13})},$$
$$s_2^2 = \frac{1}{1 - c_{13}}. \tag{119}$$

Here, $c_{ijk...} \equiv c_i + c_j + c_k + ...$ Besides, it is demanded that the energy density of each mode be positive.

2. **Primordial nucleosynthesis** – The expansion rate of the primordial Universe, determined by the cosmological gravitational constant $G_c = G/(1+8\pi G\beta)$, cannot differ by much from Newton's constant $G_N = G/\sigma$; namely,

$$\left|\frac{G_c}{G_N} - 1\right| \leq \frac{1}{8}. \tag{120}$$

3. **Gravitational Cherenkov radiation** – In order to prevent that very high energy particles loose energy by emission of gravitational modes, the mode velocities must satisfy the constraint

$$s_i^2 - 1 > -10^{-15}, \quad i \in \{0, 1, 2\}. \tag{121}$$

4. **PPN parameters** – In the weak field limit, the AE theory distinguishes itself from the General Relativity by the parameters α_1 and α_2, which quantify the effects of having a preferred referential. Observations within the solar system impose that

$$|\alpha_1| \leq 10^{-4} \text{ and } |\alpha_2| \leq 10^{-7}, \tag{122}$$

in which

$$\alpha_1 = -\frac{8(c_3^2 + c_1 c_4)}{2c_1 - c_1^2 + c_3^2}, \tag{123}$$

$$\alpha_2 = \frac{\alpha_1}{2} - \frac{(c_1 + 2c_3 - c_4)(2c_1 + 3c_2 + c_3 + c_4)}{c_{123}(2 - c_{14})}. \tag{124}$$

5. **Event GW170817** – The detection of gravitational waves imposes a strong constraint on the combination $c_{13} = c_1 + c_3$; namely,

$$|c_{13}| < 10^{-15}. \tag{125}$$

Two families of parameters which satisfy those conditions simultaneously are identified in the literature (cf. [54] and Eq. (23) of [55]). The values we have adopted in our work, $\beta = 0{,}27$ and $\sigma = 0{,}9999$, have been chosen precisely for their fitting into those allowed ranges. In particular,

- $\sigma = 0{,}9999$ imply $c_{14} = 0{,}0002$, which is a sufficiently small value so as to guarantee that α_1 and α_2 be neglectable, as imposed by the observations within the solar system.
- By combining $\beta = 0{,}27$ with the constraint $|c_{13}| < 10^{-15}$ (which enforces $c_3 \approx -c_1$), one obtains $c_2 \approx \beta/3 = 0{,}09$. This value is in the range $c_{14} \leq c_2 \leq 0{,}095$ predicted in case (i) of Eq. (23) [55], thus ensuring its consistency with the remaining constraints (positive energies, real velocities, etc.).

Therefore, choosing $\beta = 0{,}27$ and $\sigma = 0{,}9999$ not only satisfies all theoretical and observational constraints, but also allows one to explore numerically, in a realistic manner, the cosmological consequences of breaking the Lorentz symmetry in the context of the EA theory.

C Numerical solution of the Wheeler–DeWitt equation

In order to solve the Wheeler–deWitt Eq. (21) numerically, we have used the finite differences method in the Crank-Nicolson scheme. By discretizing a time-dependent Schrodinger-type equation one obtains the evolution equation of $\Psi(a, \tau)$ as

$$\Psi_{i,\,n+1} = \left(1 + \frac{i dt}{2\hbar}\hat{H}\right)^{-1}\left(1 - \frac{i dt}{2\hbar}\hat{H}\right)\Psi_{i,\,n} \tag{126}$$

in which i and n refer to the spatial and time discretization, respectively, illustrated in Fig. 19.

An interesting aspect of the Crank-Nicolson method is its unconditional stability and unitarity, for hermitian Hamiltonians discretized in a consistent way, as discussed by Iitaka [56] and Teukolsky [57]. Considering a Hamiltonian of the form

$$\hat{H} = -\frac{\partial^2}{\partial a^2} + V(a), \tag{127}$$

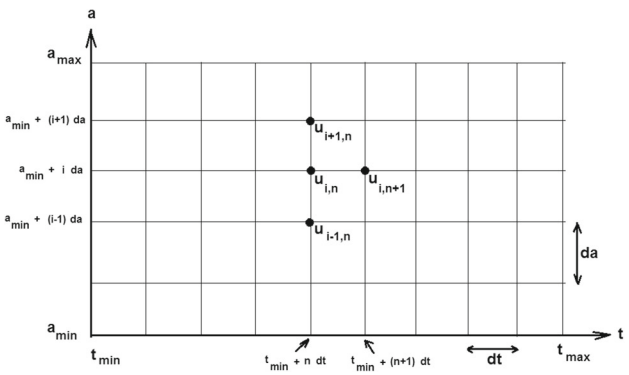

Fig. 19 Spatial and time discretization of some function $u(a, t)$, in the Crank-Nicolson scheme. The spatial interval $[a_{min}, a_{max}]$ is divided in subintervals of equal amplitude da, whereas the time interval $[t_{min}, t_{max}]$ is divided in subintervals of equal amplitude dt. The function at each point of the grid of coordinates $u(a_{min} + i\ da, t_{min} + n\ dt)$ is mapped into a matrix element $u_{i,n}$, in which (i, n) are integers

one obtains (from the spatial discretization of the second-order spatial derivative)

$$\hat{H}\Psi = -\frac{\hbar^2}{2m}\left(\frac{\Psi_{i+1,n} - 2\Psi_{i,n} + \Psi_{i-1,n}}{dx^2}\right) + V(x_i)\Psi_{i,n}, \tag{128}$$

so that the discretized Hamiltonian operator can be represented as a tridiagonal matrix,

$$\hat{H} = \begin{pmatrix} V(x_1) + \frac{\hbar^2}{mdx^2} & -\frac{\hbar^2}{2mdx^2} & 0 & 0 & \dots & 0 \\ -\frac{\hbar^2}{2mdx^2} & V(x_2) + \frac{\hbar^2}{mdx^2} & -\frac{\hbar^2}{2mdx^2} & 0 & \dots & 0 \\ 0 & -\frac{\hbar^2}{2mdx^2} & V(x_3) + \frac{\hbar^2}{mdx^2} & -\frac{\hbar^2}{2mdx^2} & \dots & 0 \\ \vdots & \dots & \dots & \dots & \ddots & 0 \\ 0 & 0 & 0 & \dots & -\frac{\hbar^2}{2mdx^2} & V(x_{n-1}) + \frac{\hbar^2}{mdx^2} \end{pmatrix}. \tag{129}$$

The initial condition used in this work, Eq. (24), is of the form

$$\Psi_0(a) = C\, a\, e^{-Ba^2}, \tag{130}$$

in which $\{C, B\}$ are real constants and $B > 0$. This form automatically satisfies the boundary conditions $\Psi_0(0) = 0$ and $\lim_{a\to+\infty} \Psi_0(a) = 0$. The constant C is determined by imposing that the norm of $\Psi_0(0)$ be unitary,

$$\int_0^\infty |\psi_0(a)|^2\, da = 1. \tag{131}$$

In its turn, the constant B can be related to the (physically meaningful) average kinetic energy $\overline{E}$,

$$\overline{E} = \int_0^\infty \psi_0^\star(a)\left(-\frac{\partial^2}{\partial a^2}\right)\psi_0(a)\, da. \tag{132}$$

By imposing those conditions, one obtains the normalized form of the initial wave function (24),

$$\psi_0(a) = 2.481612957 \cdot \left(\frac{m^3\overline{E}^3}{\pi}\right)^{1/4} \cdot a e^{-\frac{2m\overline{E}a^2}{3}}, \tag{133}$$

in which m is the parameter defined in (9).

The evolution of the wave package was calculated until it reached the point chosen as the numerical infinite. The maximum time of evolution was selected so that the package did not return from the domain boundary, thus avoiding non-physical effects associated to the spurious reflections at that point. In other words, the calculation got interrupted as $|\Psi(a,\tau)|^2$ reached the numerical domain limit.

The deviation from unity norm of the wave function as it evolved from its initial state was numerically calculated at various time instants, being of order 10^{-13} in magnitude.

By considering different grid sizes and number of time steps, under the same numerical precision, we have observed that results are stable, indicating the numerical convergence of the scheme. Hence, the application of the Crank-Nicolson method showed unconditional stability, norm conservation and numerical robustness for the evolution of the wave package $\Psi(a,\tau)$.

In what follows, Tables 2 and 3 show the convergence test results. Here, N is the number of spatial points and T is the number of time points.

D On the self-adjointness of the Hamiltonian operator

In order to show that the Hamiltonian operator is self-adjoint, we must analyze its differential form, the domain on which it acts, and the boundary conditions which are imposed [58,59].

In the context of the Einstein-Aether quantum cosmology, the total classical Hamiltonian is given by Eq. (7),

$$H = \frac{p_a^2}{2m} + V(a) - p_T. \tag{134}$$

After the canonical quantization procedure, we obtain the Wheeler-DeWitt (WDW) equation,

$$-\frac{\partial^2\Psi(a,\tau)}{\partial a^2} + 2mV(a)\Psi(a,\tau) = i2m\frac{\partial\Psi(a,\tau)}{\partial\tau}, \tag{135}$$

in which the Hamiltonian operator acting on the spatial part (scale factor a)is defined as:

$$\hat{H} = -\frac{d^2}{da^2} + 2mV(a) \tag{136}$$

so that

$$V(a) = \frac{m\omega_k^2 a^2}{2} - \Lambda a^4 \tag{137}$$

is the potential.

For a symmetric operator to be self-adjoint, it must act on a square-integrable Hilbert space; in this model, it is

Table 2 Convergence tests for fixed time parameters and varying spatial parameters. Here, time parameters were set to $t_{max} = 1.5$, $dt = 0.0015$ and $T = 1000$

Energy	N	TP_{int}	TP_{WKB}
179.8	5000	0.0025734225276100886	0.28754272585185
179.8	8000	0.12190863237057206	0.287157989667515
179.8	10000	0.13713286103682812	0.287158814990852
179.8	15000	0.15074384681109826	0.287302624462511
179.8	20000	0.1552768420652686	0.287176422015787
179.8	25000	0.15733865081503615	0.287259181767723

Table 3 Convergence tests for fixed spatial parameters and varying time parameters. Here, the spatial parameters have been set to $x_{max} = 60$, $dx = 0.004$ and $N = 15,000$

Energy	T	TP_{int}	TP_{WKB}
179.8	800	0.13363937925350788	0.287302624462511
179.8	1000	0.13713286103682812	0.287158814990852
179.8	1200	0.15897932117276858	0.287302624462511
179.8	1300	0.16162175761861483	0.287302624462511
179.8	1500	0.16531063536173293	0.287302624462511

$L^2(0,\infty,da)$ — the space of square-integrable functions on the interval $a \in [0,\infty)$. The operator domain $D(\hat{H})$ is the set of functions $\psi(a)$ satisfying the following conditions.

1. $\psi(a)$ and $\psi'(a)$ are absolutely continuous.
2. $\psi(a) \in L^2(0,\infty)$ and $\hat{\mathcal{H}}\psi(a) \in L^2(0,\infty)$.
3. The Hartle-Hawking boundary conditions: $\Psi(0,\tau) = 0$ and $\Psi(\infty,\tau) = 0$.

An operator is symmetric if $\langle\psi|\hat{H}\phi\rangle = \langle\hat{H}\psi|\phi\rangle$. Let us compute the difference between these two terms using the definition of the inner product,

$$\Delta \equiv \langle\psi|\hat{H}\phi\rangle - \langle\hat{H}\psi|\phi\rangle = \int_0^\infty \left[\psi^\star(\hat{H}\phi) - (\hat{H}\psi)^\star\phi\right] da \tag{138}$$

Substiting $\hat{H}$, we get

$$\Delta = \int_0^\infty \left[\psi^* \left(-\frac{d^2\phi}{da^2} + 2mV\phi\right) - \left(-\frac{d^2\psi^*}{da^2} + 2mV\psi^*\right)\phi\right] da \tag{139}$$

Since the potential $V(a)$ is a real function, the terms involving the potential terms cancel out. Only the kinetic part remains,

$$\Delta = \int_0^\infty \left[-\psi^\star\frac{d^2\phi}{da^2} + \frac{d^2\psi^\star}{da^2}\phi\right] da \tag{140}$$

Using Green's identity (double integration by parts), the integrand is a total derivative,

$$\Delta = \int_0^\infty \frac{d}{da}\left[\psi'^\star\phi - \psi^\star\phi'\right] da = \left[\psi'^\star\phi - \psi^\star\phi'\right]_0^\infty \tag{141}$$

Now we apply the boundary conditions specified in the article. In the lower limit $a \to 0$, the article explicitly adopts the Hartle-Hawking condition $\Psi(0,\tau) = 0$; therefore, for any $\psi, \phi \in D(\hat{H})$, we have $\psi(0) = 0$ and $\phi(0) = 0$, which makes Δ vanish in the lower limit. In the upper limit $a \to \infty$, functions belonging to the space $L^2(0,\infty)$ must decay to zero at infinity to be integrable. Since the boundary terms vanish at both limits, we have

$$\Delta = 0 \longrightarrow \langle\psi|\hat{H}\phi\rangle = \langle\hat{H}\psi|\phi\rangle; \tag{142}$$

that is, the Hamiltonian operator $\hat{H}$ is symmetric.

Symmetry and the Dirichlet condition ($\psi(0) = 0$) are sufficient conditions for the self-adjointness of a second-order differential operator on the half-line $[0,\infty)$. The operator $-d^2/da^2$ alone has deficiency indices (1, 1) [58,59], which means it admits a family of self-adjoint extensions parameterized by a boundary condition at the origin. By choosing the Hartle-Hawking condition ($\psi(0) = 0$), the authors select the Dirichlet self-adjoint extension.

Thus, we can conclude that the Hamiltonian operator is self-adjoint because its potential part is real and its kinetic part, under the Hartle-Hawking conditions, satisfies the symmetry condition and has identical domains for the operator and its adjoint ($D(\hat{H}) = D(\hat{H}^\dagger)$). This guarantees that the expectation values computed in the article, such as $\langle a(\tau)\rangle$, are always real physical quantities.

E WKB solution and tunneling probability (TP_{WKB})

Seeking solutions to the Wheeler–DeWitt Eq. (21) of the form $\Psi(a,\tau) = \psi(a)\, e^{-iE\tau}$, one finds for $\psi(a)$ the ODE

$$\frac{d^2\psi(a)}{da^2} + [2m\,(E - V(a))]\,\psi(a) = 0, \tag{143}$$

in which $V(a)$ is the effective potential given in Eq. (8). In what follows we will use the WKB approximation to solve Eq. (143), and then use that solution to calculate the tunneling probabilities through the potential barrier $V(a)$ [48,60–62].

The approximate solution for (143) is

$$\psi(a) = \begin{cases} \frac{A}{\sqrt{K(a)}} \exp\left(i\int_{a_{ltp}}^{a} K(a)da\right) + \frac{B}{\sqrt{K(a)}} \exp\left(-i\int_{a_{ltp}}^{a} K(a)da\right), & \text{for } a \le a_{ltp}; \\ \frac{C}{\sqrt{k(a)}} \exp\left(-\int_{a_{ltp}}^{a} k(a)da\right) + \frac{D}{\sqrt{k(a)}} \exp\left(\int_{a_{ltp}}^{a} k(a)da\right), & \text{for } a_{ltp} \le a \le a_{rtp}; \\ \frac{F}{\sqrt{K(a)}} \exp\left(i\int_{a_{rtp}}^{a} K(a)da\right) + \frac{G}{\sqrt{K(a)}} \exp\left(-i\int_{a_{rtp}}^{a} K(a)da\right), & \text{for } a_{rtp} \le a. \end{cases} \tag{144}$$

Here, a_{ltp} and a_{rtp} are the left and right turning points of the barrier, respectively; that is, points in which $E = V(a)$, so that $a_{ltp} \le a_{rtp}$. Furthermore,

$$\begin{cases} K(a) = \sqrt{2m\,(E - V(a))} & \text{for } E > V, \\ k(a) = \sqrt{2m\,(V(a) - E)} & \text{for } E < V. \end{cases} \tag{145}$$

The coefficient A is associated to the incident wave moving from the origin towards the left side of the barrier, and B to its reflection by barrier. Likewise, F can be associated to the transmited wave that emerges from the right side of the barrier, and G to the wave moving from infinity towards the right side of the barrier. In matrix notation, those coefficients are related by

$$\begin{pmatrix} A \\ B \end{pmatrix} = \begin{pmatrix} 2\theta + \frac{1}{2\theta} & i\left(2\theta - \frac{1}{2\theta}\right) \\ -i\left(2\theta - \frac{1}{2\theta}\right) & 2\theta + \frac{1}{2\theta} \end{pmatrix} \begin{pmatrix} F \\ G \end{pmatrix}, \tag{146}$$

in which the parameter θ is related to the height and length of the barrier,

$$\theta = \exp\left(\int_{a_{ltp}}^{a_{rtp}} k(a)da\right). \tag{147}$$

Considering that no wave is coming from the right (i.e., letting $G = 0$), the transmission coefficient, or tunneling probability can be obtained,

$$TP_{WKB} = \frac{|F|^2}{|A|^2}. \tag{148}$$

From (146),

$$A = \frac{1}{2}\left(2\theta + \frac{1}{2\theta}\right) F, \tag{149}$$

one can rewrite

$$TP_{WKB} = \frac{|F|^2}{|A|^2} = \frac{4}{\left(2\theta + \frac{1}{2\theta}\right)^2}. \tag{150}$$

References

1. J.A. Halliwell, *Quantum cosmology and baby Universes* (World Scientific, Singapore, 1991)
2. M. Bojowald, Quantum cosmology: a Review. Rep. Prog. Phys. **78**, 023901 (2015). arXiv:1501.04899 [gr-qc]
3. P.V. Moniz, Quantum Cosmology - The Supersymmetric Perspective, in Fundamentals. (Lecture Notes in Physics, vol. 1, (Springer, Berlin, 2010),
4. R. Arnowitt, S. Deser e C.W. Misner. Gravitation: An Introduction to Current Research. New York: Wiley, (1962)
5. B.S. DeWitt, Phys. Rev. **160**, 1113 (1967)
6. Wheeler, J. A. Superspace and the nature of quantum geometrodynamics. Batelle Rencontres: 1967 Lectures in Mathematics and Physics. Ed C. DeWitt and J.A. Wheeler. (1968)
7. G.A. Monerat et al., Dynamics of the early Universe and the initial conditions for inflation in a model with radiation and a Chaplygin gas. Physical Review D-Particles, Fields, Gravitation, and Cosmology **76**(2), 024017 (2007). https://doi.org/10.1103/PhysRevD.76.024017
8. G.A. Monerat et al., The dynamics of the early Universe in a model with radiation and a generalized chaplygin gas-early Universe with radiation and a generalized chaplygin gas. The European Physical Journal Plus **136**(1), 34 (2021). https://doi.org/10.1140/epjp/s13360-020-00996-3
9. D. He, D. Gao, Q.-Y. Cai, Spontaneous creation of the Universe from nothing. Physical Review D **89**(8), 083510 (2014). https://doi.org/10.1103/PhysRevD.89.083510
10. M. Koussour, N. Myrzakulov, Bouncing cosmologies and stability analysis in symmetric teleparallel $f(Q)$ gravity. Eur. Phys. J. Plus **139**, 799 (2024)
11. S.D. Odintsov, V.K. Oikonomou, Power-law $F(R)$ gravity as deformations to Starobinsky inflation in view of ACT. Phys. Lett. B **870**, 139907 (2025)

12. K. Esmakhanova et al., Dark energy in some integrable and nonintegrablefrw cosmological models. International Journal of Modern Physics D **20**(12), 2419–2446 (2011)
13. D. Mattingly, Causal sets and conservation laws in tests of Lorentz symmetry. Physical Review D-Particles, Fields, Gravitation, and Cosmology **77**(12), 125021 (2008). https://doi.org/10.1103/PhysRevD.77.125021
14. T. Jacobson, D. Mattubgly, Phys. Re. D 64(2), (2001)
15. T. Jacobson, Einstein-Aether gravity: a status report (2008), arXiv:0801.1547
16. S.M. Carroll, E. Lim, Phys. Rev. D **70**, 123525 (2004)
17. E. Lim, Phys. Rev. D **71**, 063504 (2005)
18. S.M. Carroll, J. Shu. Phys. Rev. D **73**, 103515 (2006)
19. M. Koussour, A.H.A. Alfedeel, S. Muminov, J. Rayimbaev, Observational constraints on viscous cosmology in $f(T, Lm)$ gravity. J. High Energy Astrophysics **52**, 100578 (2026)
20. S.H. Shekh, A.K. Yadav, A. Pradhan, N. Ahmad, $f(R, \Sigma, T)$ gravity and cosmic acceleration: a comprehensive analysis of physical and kinematical parameters. Nucl. Phys. B **1022**, 117245 (2026)
21. S.H. Shekh et al., Observational Constraints on $F(T, T_G)$ Gravity with Hubble's Parametrization. Symmetry **15**, 321 (2023)
22. M. Koussour, N. Myrzakulov, M.K.M. Ali, Exploring Universe acceleration through observational constraints via Hubble parameter reconstruction. J. High Energy Astrophysics **42**, 96–103 (2024)
23. M. Khodadi, E.N. Saridakis, Einstein-Aether gravity in the light of event horizon telescope observations of M87*. Phys. Dark Universe **32**, 100835 (2021). https://doi.org/10.1016/j.dark.2021.100835
24. M. Bairagi, Parametrizations of dark energy model in the background of non-canonical scalar field in Einstein-Aether Gravity. Phys. Dark Universe **39**, 101158 (2023). https://doi.org/10.1016/j.dark.2022.101158
25. A.H. Bokhari, J. Rayimbaev, B. Ahmedov, Radio loudness and spindown of pulsars in Einstein-Aether gravity. Phys. Dark Universe **34**, 100901 (2021). https://doi.org/10.1016/j.dark.2021.100901
26. A. Adam, P. Figueras, T. Jacobson, T. Wiseman, Rotating black holes in Einstein-Aether theory. Class. Quantum Gravity **39**, 125001 (2022). https://doi.org/10.1088/1361-6382/ac5053
27. K. Lin, W.-L. Qian, Echoes of axial gravitational perturbations in stars of uniform density. Chin. Phys. C **47**(8), 085101 (2023). https://doi.org/10.1088/1674-1137/acd681
28. F. Taherasghari, C.M. Will, Compact binary systems in Einstein-Aether gravity. II. Radiation reaction to 2.5 post-Newtonian order. Physical Review D 112(2), 024013 (2025). doi: 10.1103/7px1-q8ld
29. S. Jalalzadeh, A. Mohammadi, D. Demir, "A quantum cosmology approach to cosmic coincidence and inflation". Physics of the Dark Universe, 40, (2023). doi: https://doi.org/10.1016/j.dark.2023.101227
30. A.G. Riess, A.V. Filippenko, P. Challis, A. Clocchiatti, A. Diercks, P.M. Garnavich, R.L. Gilliland, C.J. Hogan, S. Jha, R.P. Kirshner, "Observational Evidence from Supernovae for an Accelerating Universe and a Cosmological Constant". The Astronomical Journal, 116(3), (1998). doi: https://doi.org/10.1086/300499
31. J.A. Frieman, M.S. Turner, D. Huterer, Dark energy and the accelerating Universe. Annu. Rev. Astron. Astrophys. **46**(1), 385–432 (2008). https://doi.org/10.1146/annurev.astro.46.060407.145243
32. D. Sorini, J.A. Peacock, L. Lombriser, The impact of the cosmological constant on past and future star formation. Mon. Not. R. Astron. Soc. **535**(2), 1449–1474 (2024). https://doi.org/10.1093/mnras/stae2236
33. S. Perlmutter, G. Aldering, G. Goldhaber, R. A. Knop, P. Nugent, P. G. Castro, S. Deustua, S. Fabbro, A. Goobar, D.E. Groom, "Measurements of and from 42 High-Redshift Super- novae". The Astrophysical Journal, 517(2). doi: https://doi.org/10.1086/307221.
34. T. Jacobson, Einstein-Aether gravity: a status report (2008), arXiv:0801.1547
35. B.F. Schutz, Perfect fluids in General Relativity: Velocity potentials and a variational principle. Phys. Rev. D **2**, 2762–2773 (1970)
36. B.F. Schutz, Hamiltonian theory of a relativistic perfect fluid. Phys. Rev. D **4**, 3559–3566 (1971)
37. F.G. Alvarenga, R.G. Furtado, R. Fracalossi, S.V.B. Gonçalves, Braz. J. Phys. **47**, 96 (2016)
38. M.S. Turner, (2022–09-26). "The Road to Precision Cosmology". Annual Review of Nuclear and Particle Science. 72 (1): 1–35. doi: https://doi.org/10.1146/annurev-nucl-111119-041046
39. G.W. Gibbons, S.W. Hawking, S.T.C. Siklos, "The Very early Universe: proceedings of the Nuffield workshop, Cambridge, 21 June to 9 July, 1982." Very Early Universe (1983)
40. A. Achúcarro et al., "Inflation: theory and observations." arXiv preprint arXiv:2203.08128 (2022). https://doi.org/10.48550/arXiv.2203.08128
41. S. Weinberg, *Cosmology* (Oxford University Press, New York, 2008)
42. M. Livio, A.G. Riess, Measuring the Hubble constant. Phys. Today **66**(10), 41–47 (2013)
43. E. Hubble, A relation between distance and radial velocity among extra-galactic nebulae. Proc. Natl. Acad. Sci. **15**(3), 168–173 (1929)
44. D. Camarena, V. Marra, Local determination of the Hubble constant and the deceleration parameter. Phys. Review Research **2**(1), 013028 (2020)
45. B.S. DeWitt, Phys. Rev. **160**, 1113 (1967)
46. P.A.M. Dirac, *Lectures on Quantum Mechanics* (Yeshiva University Press, New York, 1964)
47. J.B. Hartle, S.W. Hawking, Phys. Rev. D **28**, 2960 (1983)
48. C. Júnior, A. Oliveira et al., Birth of an Isotropic and Homogeneous Universe with a Running Cosmological Constant. Universe **11**(9), 310 (2025). https://doi.org/10.3390/Universe11090310
49. A. de Barros, J., et al., "Tunneling probability for the birth of an asymptotically de Sitter Universe." Physical Review D-Particles, Fields, Gravitation, and Cosmology 75(10), 104004 (2007). doi: https://doi.org/10.1103/PhysRevD.75.104004
50. G.A. Monerat, F.G. Alvarenga, S.V.B. Gonçalves, G. Oliveira-Neto, C.G.M. Santos, E.V. Corrêa Silva, Eur. Phys. J. Plus, 137:117, doi: 10.1140/epjp/s13360-021-02316-9 (2022)
51. H. Everett, III. The Many-Worlds Interpretation of Quantum Mechanics, ed. by B. S. DeWitt and N. Graham (Princeton University Press, Princeton, 1973)
52. F.J. Tipler, Phys. Rep. **137**, 231 (1986)
53. F.G. Alvarenga et al., Observational constraints on the quantum Einstein-Aether model. Eur. Phys. J. Plus **138**, 975 (2023). https://doi.org/10.1140/epjp/s13360-023-04615-9
54. J. Oost, S. Mukohyama, A. Wang, Phys. Rev. D 97(12), (2018)
55. F.G. Alvarenga et al., Eur. Phys. J. Plus **138**, 975 (2023)
56. T. Iitaka, Solving the time-dependent Schrödinger equation numerically. Phys. Rev. E **49**, 4684 (1994)
57. S.A. Teukolsky, Stability of the iterated Crank-Nicholson method in numerical relativity. Phys. Rev. D **61**, 087501 (2000)
58. M. Reed, B. Simon, *Methods of Modern Mathematical Physics*, vol. II (Academic Press, New York, 1975)
59. N.A. Lemos, Convite à Física Matemática. São Paulo: Ed. Livraria da Física, (2013)
60. E. Merzbacher, Quantum Mechanics. 3rd ed. (John Wiley and Sons Inc, New York, 1998), Chap. 7
61. A.O. Castro Júnior, G. Oliveira-Neto, G.A. Monerat, "Primordial dust Universe in the Hořava-Lifshitz theory." Modern Physics Letters A 39(23n24), 2450112 (2024). https://doi.org/10.1142/S0217732324501128
62. A.O. Castro Júnior, G. Oliveira-Neto, G. A. Monerat, "The initial moments of a Hořava-Lifshitz cosmological model." General Relativity and Gravitation 56(10), 125 (2024). doi: https://doi.org/10.1007/s10714-024-03310-z